Towards the Development of an Autonomous System for Driver's Drowsiness Detection and Alertness Using a High-Fidelity Driving Simulator

by

Riaz Minhas

A Dissertation Submitted to the
Graduate School of Sciences and Engineering
in Partial Fulfillment of the Requirements for
the Degree of

Master of Science

in

Mechanical Engineering

June 10, 2024

Towards the Development of an Autonomous System for Driver's Drowsiness Detection and Alertness Using a High-Fidelity Driving Simulator

Koç University

Graduate School of Sciences and Engineering

This is to certify that I have examined this copy of a master's thesis by

Riaz Minhas

and have found that it is complete and satisfactory in all respects,
and that any and all revisions required by the final
examining committee have been made.

Committee Members:

Asst. Prof. Beren Semiz Gürsoy (Advisor)

Prof. Mehmet Burçin Ünlü

Asst. Prof. Levent Beker

Date: June 10, 2024

To my family and friends, especially to my loving mother and my spouse for their continuous support and prayers, and to my siblings for always standing up for me, this thesis is dedicated to all of you.

ABSTRACT

Towards the Development of an Autonomous System for Driver's Drowsiness Detection and Alertness Using a High-Fidelity Driving Simulator

Riaz Minhas

Master of Science in Mechanical Engineering

June 10, 2024

Precise quantification of microsleep (MS) resulting from sleep-disorder and drowsiness rising from insufficient rest in obstructive sleep apnea (OSA) drivers is crucial for preventing accidents. In this work, we propose three methodologies: (i) quantifying MS episodes by correlating driving simulator events with electroencephalography (EEG) patterns; (ii) detecting drowsiness by associating EEG patterns with visual-based scoring through adaptive thresholding for eye-aspect-ratio using OpenCV for face detection and Dlib for eye detection from video recordings; and (iii) optimizing EEG channels and features for their usability in wearable devices. We also propose an autonomous real-time drowsiness detection and alert system for actual bus drivers, aiming to alert drivers through vibrations produced by an electro-pneumatic vibrator located at the back side of the driver's seat and integrated with the existing tire inflation system. Fifty drivers diagnosed with OSA participated in a 50-minute driving simulation wearing six-channel EEG electrodes, while a frontal camera recorded their facial expressions. The first technique identified 970 out-of-road (OOR) events where the wheel and boundary contact lasted $\geq$ 1 second, and 1020 on-road (OR) events where the wheel and boundary disconnection lasted $\geq$ 1 second. Applying discrete wavelet transform, theta/alpha ratios were calculated for each event. We classified OOR events with higher theta/alpha ratio compared to neighboring OR episodes as true MS and those with lower ratio as false MS. Comparative analysis focused on frontal brain matched 791 of 970 OOR events with true MS episodes, outperforming other brain regions. Extending our analysis to all channels showed an even higher matching, correlating 923 (95.15%) of 970 OOR events with true MS episodes. We also quantified MS duration, with 95% of total episodes lasting between 1 to 15 seconds, and pioneered a robust correlation ($r = 0.8913$, $p<0.001$) between maximum drowsiness level and MS density. The second technique identified 453 drowsy (PERCLOS $\geq$ 0.3 or CLOSDUR $\geq$ 2 seconds) and 474 wakeful (PERCLOS $<$ 0.3 and CLOSDUR $<$ 2 seconds) episodes. By applying discrete wavelet transform, we derived ten EEG features and correlated them with visual-based episodes using various comparative criteria. We assessed that the theta-to-alpha ratio exhibited robust mapping (94.7%) with visual-based scoring, followed by the delta-to-alpha ratio (87.2%) and delta-to-theta ratio (86.7%) while considering all channels together. Notably, the frontal area (86.4%) and channel F4 (75.4%) aligned most episodes with theta-to-alpha-ratio, while the frontal, occipital regions, particularly individual channels F4 and O2, displayed superior alignment across multiple features. The third technique normalized ten EEG features for each visual-based episode, then computed seven different thresholding techniques to identify the most consistent method across subjects. Episodes were classified as either drowsy or wakeful based on feature-dependent criteria, evaluating whether their normalized values were above or below a specific threshold. We paired the EEG features into 45 combinations to determine the ideal pair in classifying each episode,

in line with visual scoring. Among these, the pairing of PSD alpha and PSD theta in channels F4 and O2 achieved average coverages of 96.1% and 95%, respectively, with corresponding accuracies of 95.4% and 94.7%. These coverages slightly surpassed the results obtained using six channels and a single feature, with an increase of 1.47% for F4 and 0.32% for O2. Lastly, we presented a novel approach towards the development of real-time drowsiness detection and alert system for an actual bus. In conclusion, our work could potentially be employed to assess fitness-to-drive in OSA patients using a driving simulator, reduce hardware and computational demands, and pave the way for an effective real-time drowsiness detection and alert system for actual bus drivers.

ÖZETÇE

Yüksek Hassasiyetli Sürüş Simülatörü Kullanılarak Sürücünün Uykululuk Tespiti ve Uyanıklığı için Otonom Bir Sistemin Geliştirilmesine Doğru

Riaz Minhas

Makine Mühendisliği Yüksek Lisansı

10 Haziran 2024

Obstrüktif uyku apnesi (OSA) olan sürücülerde uyku bozukluğu ve yetersiz dinlenme sonucu ortaya çıkan uyuşukluğun neden olduğu mikro uykunun (MS) hassas ölçümü, kazaların önlenmesi açısından çok önemlidir. Bu doğrultuda üç metodoloji öneriyoruz: (i) sürüş simülatörü verilerini elektroensefalografi (EEG) modelleri ile ilişkilendirerek MS epizodlarının ölçülmesi; (ii) yüz tespiti için OpenCV ve video kayıtlarından göz tespiti için Dlib kullanılması, göz-en-boy oranının uyarlanabilir eşikleme yolu ile hesaplanması ve EEG modellerini görsel tabanlı puanlamayla ilişkilendirerek uyuşukluğun tespit edilmesi; ve (iii) giyilebilir sistemlerde kullanılmak üzere EEG kanallarının ve özniteliklerinin optimize edilmesi. Ayrıca, gerçek otobüs sürücüleri için, sürücü koltuğunun arka tarafında bulunan ve mevcut lastik şişirme sistemi ile entegre olan bir elektro-pnömatik vibratörün ürettiği titreşimler aracılığıyla sürücüleri uyarmayı amaçlayan, otonom, gerçek zamanlı uykululuk tespit ve uyarı sistemi de öneriyoruz. Çalışmamızda, OSA teşhisi konan elli sürücü, altı kanallı EEG elektrotları barındıran 50 dakikalık bir sürüş simülasyonuna katılırken, bir ön kamera ile yüz ifadeleri kaydedildi. İlk teknik, tekerlek ve şerit temasının ≥ 1 saniye sürdüğü 970 yol dışı (OOR) olayı ve tekerlek ve şerit bağlantısının kesilmesinin ≥ 1 saniye sürdüğü 1020 yol içi (OR) olayı tanımladı. Analizlerimizde, ayrık dalgacık dönüşümü uygulayarak her olay için teta/alfa oranlarını hesapladık. Komşu OR epizotlarına kıyasla daha yüksek teta/alfa oranına sahip OOR olaylarını gerçek MS, daha düşük orana sahip olanları ise yanlış MS olarak sınıflandırdık. Ön beyne odaklanan karşılaştırmalı analiz, 970 OOR olayından 791'ini gerçek MS epizodlarıyla eşleştirerek diğer beyin bölgelerinden daha iyi performans gösterdi. Analizimizi tüm kanallara genişlettiğimizde, 970 OOR olayının 923'ünü (%95,15) gerçek MS epizodlarıyla ilişkilendirerek daha da yüksek bir eşleşme elde ettik. Ayrıca toplam epizotların %95'inin 1 ila 15 saniye arasında sürdüğü MS süresini de ölçtük ve maksimum uyuşukluk düzeyi ile MS yoğunluğu arasında güçlü bir korelasyon ($r = 0,8913$, $p<0,001$) gözlemledik. İkinci teknik, 453 uykulu (PERCLOS ≥ 0,3 veya CLOSDUR ≥ 2 saniye) ve 474 uyanık (PERCLOS < 0,3 ve CLOSDUR < 2 saniye) epizodu tanımladı. Ayrık dalgacık dönüşümü uygulayarak on EEG özniteliği türettik ve bunları çeşitli karşılaştırma kriterleri kullanarak görsel tabanlı epizodlarla ilişkilendirdik. Tüm kanalları bir arada kullandığımızda, teta-alfa oranının görsel tabanlı puanlamayla güçlü ilişki (%94,7) gösterdiğini, bunu delta-alfa oranının (%87,2) ve delta-teta oranının (%86,7) izlediğini değerlendirdik. Özellikle, frontal (%86,4) ve F4 kanalı (%75,4) kullanıldığında çoğu epizod teta-alfa oranı ile yüksek ilişki gösterirken; frontal ve oksipital bölgeler (özellikle bireysel F4 ve O2 kanalları), birçok öznitelikte üstün ilişki sergiledi. Üçüncü teknikte, her görsel tabanlı epizod için on EEG özelliği normalize edildi, ardından katılımcılar arasında en tutarlı yöntemi belirlemek için yedi farklı eşikleme tekniği hesaplandı. Epizodlar, özelliğe bağlı kriterlere göre uykulu veya uyanık olarak sınıflandırıldı ve normalleştirilmiş değerlerin belirli bir eşiğin üstünde veya altında olup olmadığı incelendi. Her segmenti görsel puanlamaya göre sınıflandırmak için ideal

çifti belirlemek amacıyla EEG özelliklerini 45 eşleştirilmiş kombinasyon halinde birleştirdik. Bunlar arasında, F4 ve O2 kanallarındaki PSD alfa ve PSD teta kombinasyonu, sırasıyla %96,1 ve %95'lik ortalama kapsama elde etti ve karşılık gelen doğruluk oranı %95,4 ve %94,7 oldu. Bu kapsamlar, F4 için %1,47 ve O2 için %0,32'lik bir artışla, altı kanal ve tek bir özellik kullanılarak elde edilen sonuçlara kıyasla kısmen daha yüksekti. Son olarak, gerçek bir otobüs için gerçek zamanlı uykululuk tespit ve uyarı sisteminin geliştirilmesine yönelik yeni bir yaklaşım sunduk. Sonuç olarak, çalışmamız, bir sürüş simülatörü kullanarak OSA hastalarında araç sürmeye uygunluğu değerlendirmek, donanım ve hesaplama taleplerini azaltmak ve gerçek otobüs sürücüleri için etkili bir gerçek zamanlı uykululuk tespiti ve uyarı sisteminin önünü açmak için potansiyel olarak kullanılabilir.

AKNOWLEDGEMENTS

I am profoundly grateful to my advisor, Assistant Professor Beren Semiz Gürsoy, for her unwavering support and dedication throughout my master's program. Her guidance was crucial in the completion of this thesis, and I owe its success to her invaluable assistance.

I also extend my thanks to Assistant Professors Levent Beker and Professor Mehmet Burcin Unlu for agreeing to serve as jury members to review my thesis work and for providing invaluable feedback.

I would like to express my appreciation to Prof. Dr. Yüksel Peker and Prof. Cigdem Eroglu Erdem for their invaluable guidance in the clinical and image processing sections of my thesis work.

I am grateful to Asim Senyuva, the co-founder of ANGRUP Software Technologies & Metatiative Inc., for his support during the development of the experimental setup. Furthermore, I appreciate the services and facilities provided by the Koç University Research Center for Translational Medicine (KUTTAM).

I acknowledge the valuable contributions of Nur Yasin Peker, Mustafa Abdullah Hakkoz, Semih Arbatli, and Yeliz Celik to my research work.

Additionally, I would like to express my gratitude to my senior colleagues at my workplace in Pakistan, particularly Dr. Faizul Hassan, Mr. Muhammad Jamil, and Mr. Wilayat Badshah, for providing me with the opportunity to pursue my master's degree abroad.

I am also thankful to my parents and siblings for their constant motivation. I extend my deepest appreciation to my loving spouse, Dr. Fareeha Kanwal, for single-handedly taking care of our kids during my master's studies in Turkey. I would not have completed this landmark without her unwavering and invaluable support.

TABLE OF CONTENTS

LIST OF TABLES

LIST OF FIGURES

ABBREVIATIONS

MS	Microsleep
DTS	Driver Training Simulator
OOR	Out of Road
OR	On Road
EEG	Electroencephalography
DD	Drowsiness Detection
IP	Image Processing
PSD	Power Spectral Density
DWT	Discrete Wavelet Transform
SA	Sleep Apnea
OSA	Obstructive Sleep Apnea
CSA	Central Sleep Apnea
AHI	Apnea Hypopnea Index
ODI	Oxygen Desaturation Index
REM	Rapid Eye Movement
EDS	Excessive Daytime Sleepiness
MWT	Maintenance of Wakefulness Test
MSLT	Multiple Sleep Latency Test
EAR	Eye Aspect Ratio
PERCLOS	Percent of Eye Closure over Time in Seconds
CLOSDUR	Duration for Eye Closure
MDL	Maximum Drowsiness Level
IR	Identification Rate
MIR	Mean Identification Rate
CMIR	Combined Mean Identification Rate
EPR	Event Related Pattern
IQR	Interquartile Range
ASM	Alert System Module
TIS	Tire Inflation System
EPS	Electro-Pneumatic System

Chapter 1:
INTRODUCTION

Disclaimer: This chapter (1) has been adapted from the following articles with permission from all co-authors:
R. Minhas et al., "A Novel Approach to Quantify Microsleep in Drivers with Obstructive Sleep Apnea by Concurrent Analysis of EEG Patterns and Driving Attributes," in IEEE Journal of Biomedical and Health Informatics, vol. 28, no. 3, pp. 1341-1352, March 2024.
Minhas, R. et al., "Association of Visual-Based Signals with Electroencephalography Patterns in Enhancing the Drowsiness Detection in Drivers with Obstructive Sleep Apnea," Sensors, vol. 24, no. 9, p. 2625, 2024.

1.1 Motivation

Sleep apnea (SA) is a common disorder characterized by breathing interruptions during sleep [1][2]. There are two main types: (1) Obstructive Sleep Apnea (OSA), which occurs when the airway at the back of the throat narrows or becomes blocked during sleep, leading to decreased oxygen levels in the blood and disrupted sleep [3][4][5], and (2) Central Sleep Apnea (CSA), which results from communication issues between the brain and the muscles that control breathing, causing temporary breathing pauses [6][7]. OSA is typically diagnosed with an Apnea Hypopnea Index (AHI) exceeding five events per hour of sleep and affects approximately 10% to 30% of adults in the United States [8][9]. In contrast, CSA is less common, with a prevalence rate of around 1% [10]. OSA is associated with a repetitive cycle characterized by loud snoring, disruptions in rapid eye movement (REM) sleep, and frequent awakenings during the night [11]. These disruptions in sleep patterns contribute to symptoms such as fatigue and excessive daytime sleepiness (EDS), which can impact focus at work and driving performance [12][13].

Individuals experiencing EDS may encounter episodes of microsleep (MS) during the day. MS and drowsiness are related but not exactly the same. Drowsiness refers to a state of feeling sleepy or tired, where a person may have difficulty staying awake and alert [14]. On the other hand, MS are brief, involuntary moments of sleep or attention lapse that can happen even when a person appears awake and engaged in an activity [15]. Importantly, even well-rested individuals can experience MS episodes [16]. Figure 1.1a

depicts the common causes, effects, and consequences of MS, characterized by very short sleep episodes lasting 15 seconds or less [17][18][19]. These MS episodes are identifiable by partially closed eyes, nodding of the head, and a complete loss of visuomotor responsiveness [20][21]. Furthermore, when analyzing the brain's electrical activity using electroencephalography (EEG), MS is typically associated with reduced alpha wave (8-13 Hz) activity and increased theta wave (4-7 Hz) activity [22]. Figure 1.1b illustrates the transition in frequency bands from alpha to theta waves in the brain.

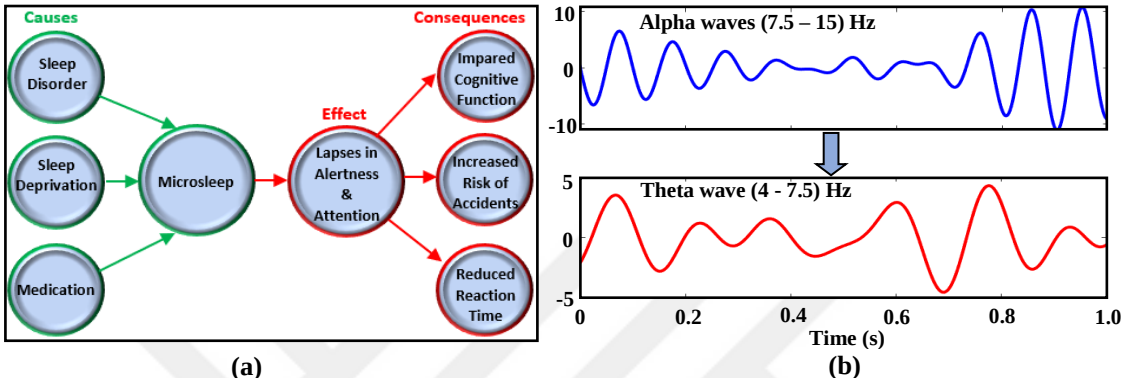

Figure 1.1: (a) Causes, effect, and consequences of microsleep (b) Shifting of alpha waves to theta waves in the brain is the onset of a microsleep.

MS and drowsiness plays a critical role in road traffic accidents, often occurring when drivers nod off at the wheel due to sleep disorders and inadequate rest, respectively [23][24]. Individuals with OSA face a two-to-seven times higher possibility of road accidents compared to the general population [25][26]. A healthy driver typically experiences a crash risk of 0.08 per person-year, whereas a driver with OSA faces a heightened risk ranging from 0.10 to 0.39 per person-year [27]. Previous instances of MS have resulted in fatal accidents with widespread consequences, leading to over 200 fatalities and more than 400 injuries in a single event [28]. According to estimates from the US National Highway Traffic Safety Administration (NHTSA), drowsiness contributes to more than 100,000 road accidents globally each year, resulting in over 800 deaths and 50,000 injuries [29]. According to the American Automobile Association (AAA), drowsy driving contributes to one-sixth of fatal traffic accidents and one-eighth of accidents requiring hospitalization for drivers or passengers [30]. These facts underscore the necessity of quantifying MS episodes and identifying drowsiness in OSA patients to evaluate their driving fitness and prevent real-world accidents.

Chapter 2:

LITERATURE REVIEW

Disclaimer: This chapter (2) has been adapted from the following articles with permission from all co-authors:

R. Minhas et al., "A Novel Approach to Quantify Microsleep in Drivers with Obstructive Sleep Apnea by Concurrent Analysis of EEG Patterns and Driving Attributes," in IEEE Journal of Biomedical and Health Informatics, vol. 28, no. 3, pp. 1341-1352, March 2024.

Minhas, R. et al., "Association of Visual-Based Signals with Electroencephalography Patterns in Enhancing the Drowsiness Detection in Drivers with Obstructive Sleep Apnea," Sensors, vol. 24, no. 9, p. 2625, 2024.

2.1 Previous Studies on Detecting MS Episodes

The availability of hospital-based diagnostic tools to assess sleep-related driving impairments is limited [17][31][32]. Evaluations using the Multiple Sleep Latency Test (MSLT) and the Maintenance of Wakefulness Test (MWT) have limitations in gauging a driver's ability to operate a vehicle as they occur in non-interactive, sleep-inducing settings that do not adequately replicate real-world driving conditions. The complex nature of driving encompasses perceptual, motor, and cognitive skills [33], rendering these tests ineffective in accurately assessing MS.

Simulated driving environments are a widely recognized approach for quantifying MS episodes and effectively mimic real-world driving conditions [34][35][36]. These environments involve three main categories of data classification: (1) physiological-based signals including EEG, EOG, EMG, and ECG [37][38][39]; (2) behavioral-based signals like eye movement [40][41], yawning [42], and head-nodding [43]; and (3) vehicle-based signals, demonstrated by steering entropy, lane deviation, and out-of-road events [44][45]. Previous research has also sought to integrate the aforementioned signals, such as combining vehicle-based signals with EEG signals to detect MS episodes, albeit with some limitations.

2.1.1 Integrating Vehicle-Based Signals with EEG Signals

One study manually identified MS episodes lasting 3-14 seconds, characterized by the transition from alpha to theta EEG activity. It also evaluated their influence on driving

performance, analyzing variables such as speed, lane-keeping, and steering control, and uncovered a notable decline in vehicle control during MS episodes [35]. In a separate study, OSA patients were compared to healthy individuals, highlighting increased lane position variability (OSA: 0.62 ± 0.36; Healthy: 0.26 ± 0.12) and a higher frequency of crashes in the OSA group (OSA: 3.1; Healthy: 0.04), which were linked to frequent MS episodes [46]. In another study, subjective ratings of sleepiness and alertness were integrated with manual EEG-verified MS episodes. The study revealed a substantial correlation between the average incidence of MS episodes and the risk of crashes ($r=0.748$, $p<0.01$) [47]. A study conducted on drivers with OSA found that there was a lane position variation of 0.16 during MS episodes, which decreased to 0.09 after an MS episode [48]. In a different study, the manual identification of MS episodes involved tracking three video streams of driving scenes and observing subjects' eye movements. This data was then correlated with electrocardiogram (ECG) patterns, which revealed a decrease in heart rate and an increase in heart rate variability during these episodes [49]. In some studies, deep learning models such as U-Time and Long Short-Term Memory Neural Network (LSTMNN) were employed to detect MS episodes initially scored manually based on EEG, electrooculogram (EOG), and eyelid closure (≥ 80%) data collected during night-sleep or MWT. These models were trained on the manually identified MS episodes and subsequently used to detect MS in simulated driving scenarios [17][50].

2.1.2 Drawbacks in Integrating Vehicle-Based Signals with EEG Signals

Studies[17][46][47] did not establish a direct correlation between MS episodes and driving performance but rather examined its overall impact. Studies[45][46][47][48] did not account for MS episodes lasting less than 3 seconds, despite a substantial portion (40%) falling within this short duration[51]. Furthermore, manual interpretation of these brief MS episodes can be challenging, susceptible to human error, and labor-intensive[17][22]. Studies utilizing personal computer-based driving simulators [46][47][49] may also be subject to reliability issues [52][53]. Moreover, studies[17][50] that train their models in non-interactive, sleep-inducing environments may face challenges in replicating the intricacies of real-world driving conditions. Driving requires a range of cognitive and psychomotor abilities that are not evaluated in MWT or MSLT paradigms, which could potentially impact the model's performance in detecting MS

during simulated driving scenarios. Additionally, these models were trained using manual scoring, and the threshold of eyelid closure ≥ 80% may not capture instances where MS occurs with open eyes[17][50][54]. Crucially, none of the preceding studies accounted for EEG channel sensitivity in the identification of MS or quantified the maximum drowsiness level (MDL).

2.1.3 A Proposed Solution to Overcome Limitations in Previous Studies

In our study, our objective is to establish a direct correlation between driving attributes and brain patterns to accurately quantify MS episodes in clinically diagnosed OSA patients. We will achieve this by employing a high-fidelity driving simulator and validating the simulator signals with EEG data, while avoiding manual scoring of MS episodes. We also aim to pinpoint the most sensitive brain region to capturing all MS episodes. This approach overcomes the limitations found in earlier research. Therefore, the primary contributions of this study to quantify MS episodes are as follows:

- We propose two distinct approaches to detect MS episodes: (i) vehicle-based (OOR and OR events), and (ii) physiological signal-based (EEG) (Chapter 3.4).
- We propose an integrated method that combines both approaches to successfully enhance the reliability of MS identification (Chapters 3.5 and 6.1).
- We conduct extensive computations on numerous parameters associated with MS, including frequency, temporal information, maximum drowsiness level, and event related patterns in the brain (Chapters 3.6, 3.8, 3.9 and 6.2, 6.4, 6.5).
- We calculate the sensitivity of different EEG channels in identifying MS episodes (Chapters 3.7 and 6.3).

2.2 Previous Studies on Detecting Drowsiness

Research underscores EEG signals as extremely efficient in promptly detecting the onset of drowsiness, outperforming both behavioral-based and vehicle-based systems [55][56][57]. Despite the behavioral-based system lagging slightly behind EEG measures in identifying the onset of drowsiness, it can detect early indicators such as eye-blinking associated with drowsiness before any lateral vehicle displacement happens [58]. As vehicle-based systems arise warnings later during the initial drowsiness phase, potentially restricting opportunities for accident avoidance, trusting solely on this technique is not

recommended. Instead, combining it with other methods for detecting driver drowsiness has proven more effective [55]. PERCLOS, a behavioral-based signal approved by the NHTSA for independent drowsiness detection, measures the duration of eyes closed at least 80 percent within one minute [59]. It can be computed via built-in algorithms in eye-tracking systems (ETS) such as SmartEye [58], or through image processing from recorded facial videos [40][41]. However, drawbacks in image processing include challenges related to video and image quality, interference from eyewear, variations in lighting conditions, and head movements, all of which can impact performance [55][57][58]. Addressing these constraints is crucial, as relying solely on image processing may lack reliability. Therefore, validating this method against established physiological signals and mitigating its limitations are essential for improving dependability in real-world scenarios.

2.2.1 Integrating Behavioral Signals with EEG Signals

Previous research has identified drowsiness using PERCLOS, although with certain limitations. For instance, one study achieved 88.9% precision by utilizing skin color identification, the Sohel edge operator for eye localization, and dynamic templates for eye tracking [40]. Another study developed a real-time application using the Viola-Jones detector, which achieved 90% accuracy through the nearest neighbor IBk and J48 decision tree algorithms [41]. Several studies have combined PERCLOS with additional behavioral parameters, including average eye closure speed [60], head movement [61], and episodes of yawning [62], thus enhancing the effectiveness of drowsiness detection. Moreover, a study [58] correlated PERCLOS-based drowsiness with neural patterns, uncovering an increase in theta and delta powers as PERCLOS levels escalated during driving tests. Study [59] employed photoplethysmography imaging (PPGI) to calculate heart rate variability (HRV) and the LF/HF ratio, achieving an accuracy of 92.5% by correlating these HRV-derived parameters with PERCLOS measurements. Furthermore, a couple of studies [63][64] combined PERCLOS with vehicle-based signals, including steering wheel movement [63] and lane position [64]. Additionally, another study [65] integrated PERCLOS with a galvanic skin response (GSR) sensor using Multi-Task Cascaded Convolutional Neural Networks (MTCNN), successfully predicting the driver's transition from an awake to a drowsy state with 91% efficacy.

2.2.2 Drawbacks in Integrating Behavioral Signals with EEG Signals

Study [40] regarded a 250-millisecond eyeblink as a sign of drowsiness, although normal blinks typically last between 100-400 milliseconds [66]. Furthermore, studies [40][41] solely depended on PERCLOS for detecting drowsiness. Studies [60][61][62] did not validate their drowsiness detection systems, which incorporated PERCLOS along with other behavioral parameters, against any physiological signals. Study [57] utilized SmartEye for PERCLOS calculation, which was acknowledged as reliable but deemed cost ineffective. A study [59] acquired PPGI from facial images, demonstrating lower accuracy when compared to traditional PPG methods. Additionally, studies [63][64] endeavored to associate PERCLOS with vehicle-based signals; however, they did not consider the potential time delay between these two types of signals. All studies except one [58] failed to address the limitations in calculating PERCLOS via image processing. Moreover, none of the studies established a direct correlation between visual-based scoring using PERCLOS and physiological signals; instead, they examined their general association. Lastly, none of the studies identified EEG channel or brain region sensitivity when correlating visual-based scoring with EEG patterns.

2.2.3 A Proposed Solution to Overcome Limitations in Previous Studies

In our study, our goal is to improve the reliability of drowsiness detection using a driving simulator in clinically diagnosed patients with OSA. Our approach involves implementing adaptive thresholding for calculating the eye-aspect-ratio (EAR) to reduce limitations associated with computing PERCLOS through image processing. Additionally, we aim to validate this method by establishing a direct correlation between instances of visual-based scoring and EEG patterns, utilizing ten distinct features. Furthermore, we assess the sensitivity of individual EEG channels and brain regions in generating this correlation. Through these measures, our approach effectively addresses the limitations encountered in previous studies. Therefore, the main contributions of this study to identify drowsiness are as follows:

- Introducing a visual-based scoring method to detect episodes of drowsiness and wakefulness using adaptive thresholding—instead of fixed thresholding—for eye-aspect-ratio computation. This method leverages Python-based OpenCV for face detection and Dlib for eye region extraction (Chapters 4.4 and 7.1).

- Proposing an integrated approach that correlates visual-based scoring with EEG patterns using ten distinct features to enhance the reliability of drowsiness detection (Chapters 4.5 & 7.1).
- Computing the sensitivity of various EEG channels and brain regions to determine the optimal electrode count for this correlation, leading to minimizing hardware requirements, enhancing wearable applications, and prioritizing user comfort. (Chapters 4.6 & 7.2).

2.3 Need for EEG Channels and EEG Features Optimization

Research underscores EEG signals as the gold standard for promptly detecting the onset of drowsiness, surpassing both behavioral and vehicle-based measures [57][58]. Although EEG systems tailored for research and medical contexts often utilize multichannel, at least 4 channels in the Multiple Sleep Latency and Maintenance of wakeful Tests, to enhance coverage, their complex assembly and prolonged application times can inadvertently lead to discomfort for users, rendering them impractical for real-world applications [67][68]. Conversely, low-cost EEG systems are quicker to install and user-friendly, but their fewer electrodes (typically up to 2) often result in lower coverage [69]-[74]. Therefore, optimizing the number of EEG channels, particularly focusing on single-channel utilization, while maintaining high coverage comparable to a multi-channel system, is crucial for addressing the constraints of real-world DD.

2.3.1 Previous Studies on EEG Channels Optimization

In one study [69], subjects' response time to lane departure events served as ground truth, leading to the development of a system based on a unipolar single EEG channel. This system utilized θ and α-based features from the occipital area (Oz), achieving 82.8% accuracy. Another study [70] used drivers' self-assessment, where they pressed a button when feeling drowsy, to develop a system based on bipolar EEG channels. This system utilized weighted θ∼β features from the temporal and parietal areas (T3 & P4 or T4 & P3), achieving 90.4% accuracy. Using the Rechtschaffen and Kales (R&K) sleep scoring standard as a reference, study [71] developed a unipolar single-channel EEG-based system and extracted α and β features from the frontal area (Fp1), achieving 81% accuracy. Furthermore, in study [72], PERCLOS was utilized as a reference, where a support vector machine-based posterior probabilistic model (SVMPPM) achieved

91.92% accuracy for the drowsiness group (91 out of 99 data sets), utilizing channels O1 and O2. Another study [73] used a prefrontal single-channel EEG device, achieving a 72.7% classification accuracy using power spectral density (PSD) with stepwise linear discriminant analysis (SWLDA) and support vector machine (SVM) models. Additionally, study [74] transformed the filtered EEG signal into a 2D spectrogram, then classified it using AlexNet with transfer learning. FP1 and T3 channels were identified as the most accurate, achieving up to 90% and 91% accuracy, respectively, in detecting drowsiness states.

2.3.2 Limitations in Previous Studies on EEG Channels Optimization

Study [69] overlooked potential delays between vehicle-generated alerts and EEG signals, as vehicle-based warnings typically occur later in the initial phase of drowsiness [58]. Study [70] relied on drivers' self-assessment for reference drowsiness, introducing subjective biases. Study [71] used manual sleep scoring based on the R&K standard, which is challenging, prone to error, and labor-intensive [52]. Additionally, its effectiveness may be compromised by epochs shorter than three seconds [35]. Study [72] employed a personal computer-based driving simulator, which may not effectively mimic real-world driving conditions [53]. Study [74] did not include a comparative analysis between their methodology and other established techniques or scoring systems for validation. None of the studies compared their optimized EEG-channel system with a multi-channel system and made efforts to optimize EEG features.

2.3.3 A Proposed Solution to Overcome Limitations in Previous Studies

In our study, we aim to use visual-based scoring to identify wakeful and drowsy episodes by integrating two metrics: PERCLOS and CLOSDUR, as a reference system. Building on our previous research [75][76], which highlighted superior alignment of channels F4 and O2 across multiple features, our EEG channel optimization focuses on these two crucial channels for accurately capturing EEG patterns associated with drowsy and wakeful episodes through optimal feature pairing. Additionally, to enhance our methodology's reliability, we will compute average combined coverage and accuracy of paired features for each channel, using comparative criteria and thresholding classification, respectively. To the best of our knowledge, this will be the first study to compare an optimized single-channel EEG system with a multichannel system, focusing

on the optimization of EEG features and suggesting that channel F4 is slightly more sensitive in detecting drowsiness patterns than channel O2. Thus, the major contributions of this study to optimize EEG channels and features are as follows:

- We propose subject-specific and EEG feature-specific classification using optimal thresholding selected from seven techniques to achieve consistent results across all features and subjects (Chapters 5.1 and 8.3).
- We evaluate combinations of EEG features, totaling 45 pairs, to assess the optimal feature pair for classifying episodes as drowsy or wakeful, corresponding to visual-based scoring (Chapters 5.1 and 8.1).
- For each channel, we compute the average coverage and accuracy for each feature within a pair, and also determine these metrics for the combined pair, across fifty subjects. We believe the similarity between average coverage and average accuracy showcasing the reliability of our methodology (Chapters 5.1 and 8.1).
- Additionally, we present the enhancement in average coverage achieved using a single channel compared to six channels (Chapters 5.1 and 8.2).

2.4 Autonomous Real-Time Drowsiness Detection and Alert System

Many previous studies on EEG-based drowsiness detection have employed a uniform detection model for all subjects [77]. However, it is widely recognized that there exists significant individual variability in EEG dynamics associated with drowsiness [78]. Therefore, we propose a real-time drowsiness detection system for an actual bus based on subject-specific pre-calculated EEG feature thresholds obtained in a simulated environment, utilizing a single channel EEG system based on our channel optimization work (Chapter 9). The system will also include an alert mechanism for the driver using a super silent electro-pneumatic vibrator installed at the back of the driver's seat. This alert mechanism will be integrated with the existing bus tire inflation system (TIS).

Chapter 3:
METHODS FOR MICROSLEEP DETECTION

3.1 Experimental Setup

The XBUS PRO Driver Training Simulator (DTS), developed by ANGRUP Co., Istanbul, Turkey, was utilized in our study at the Sleep Laboratory of Koç University Hospital in Istanbul. Figure 3. 1 depicts the overall experimental setup employed in this study. The simulator offered the choice of manual or automatic transmission to accommodate different driving preferences. It was equipped with various sensors that detected throttle usage, brake application, road departures, steering anomalies, potential traffic accidents, and lane deviations without providing indications. The simulator was housed within a soundproof cabin, ensuring a controlled environment for the participants. With a 135-degree field of view (FoV), the simulator provided a comprehensive visual perspective. Utilizing ANGRUP Software Technologies, the driving scenarios simulated within the simulator replicated a range of road conditions, such as straight segments, circular sections, and curved paths. Additionally, the scenarios included two-way traffic on a highway with low traffic to mimic a monotonous driving environment. An external device, including a 6-channel EEG device with a sampling rate of 200 Hz, was seamlessly integrated with the simulator. The EEG signals were obtained from all participants using precise electrode placements following the standardized 10-20 system [79], as shown in Figure 3. 1c. These specific electrodes (F3, F4, C3, C4, O1, and O2) were selected based on established scientific literature that has emphasized the significant correlation between EEG changes in occipital and central regions and levels of driver drowsiness [80][81]. Additionally, there is a recognized connection between variations in sustained attention and the theta and alpha frequency bands, particularly focusing on the frontal and parietal brain regions [82]. By utilizing this comprehensive electrode setup, our study effectively captured crucial neural activity patterns associated with various driving behaviors.

3.2 Human Subject Protocol and Subject Demographics

Fifty professional drivers diagnosed with OSA (AHI ≥ 5.0 events/h) based on their previous night's polysomnography results were recruited from the Sleep Laboratory for a simulator-assisted sleepiness test [83]. The study protocol was approved by the Koç University Committee on Human Research (2020.292.IRB2.083; 19 June 2020), and

Figure 3. 1: XBUS PRO driving simulator consisting of various training scenarios, camera system, voice communication system, acceleration and brake pedals, steering, automatic and manual transmission, instructor station for remote control and a variety of sensors to record the driving attributes (b) Six-channel EEG device (NOX-A1 system; Nox Medical Inc., Reykjavik, Iceland to record EEG signals at 200 Hz sampling rate (c) International 10-20 system used for the placement of EEG electrodes on the scalp of a subject (F3 and F4: frontal, C3 and C4: central, O1 and O2: occipital, M1 and M2: reference).

written informed consent was obtained from all participants. Table 3. 1 displays the demographics of all subjects. Participants were excluded from the study if they did not possess a valid driver's license, were currently experiencing acute illness, or had

consumed caffeinated beverages such as coffee and energy drinks, as well as other stimulants, within 24 hours prior to the experiment [84].

Table 3. 1: Demographics of the fifty participants. Each row displays the minimum-maximum (mean ± standard deviation) of a corresponding characteristic.

Parameters	Value
Sex	All are males
Body Mass Index (BMI)	23.8-41.9 (31.6 ± 4.1) kg / m2
Age	1-11 (6.3 ± 1.8) hour
Last night sleep hours	6.4-103.5 (31.4 ± 22.6) / hour
Apnea-Hypopnea Index (AHI)	2.0-87.8 (25.7 ± 22.2) / hour
Oxygen Desaturation Index (ODI)	23.8-41.9 (31.6 ± 4.1) kg / m2

3.3 Experimental Design

Participants who met the inclusion and exclusion criteria were scheduled for a simulated driving session between 08:00 AM and 10:00 AM. Before starting the experiment, a lab technician conducted a 10-minute training session to familiarize the drivers with the vehicle controls and provide practice scenarios involving highway driving, two-way traffic, low traffic density, and navigating a straight road with multiple turns. This initial training aimed to ensure the drivers were prepared for the subsequent simulated driving tasks, improving their overall performance and engagement. EEG electrodes were then attached to the participant, the lights in the cabin were turned off, and the door was closed. Throughout the experiment, participants were involved in a fifty-minute simulated driving session on a two-way highway, with traffic density maintained at a low level. The driving route included various sections, such as straight and curved segments, each with different speed limits, although the maximum permitted speed was capped at 62 mph (80 km/h). Integrated sensors within the simulator detected and measured any mistakes made by the driver, such as traffic accidents, sudden braking, or violations of traffic regulations like driving out of the road (OOR), changing lanes without signaling, or exceeding speed limits. These errors were recorded along with their corresponding timestamps. Figure 3. 2 provides an illustration of the experimental design used in this study.

Figure 3. 2: The experiment design commenced with the collection of clinical data from each participant, followed by the acquisition of vehicle-based parameters and EEG signals. Subsequently, the collected data was stored in relevant file formats, and a synchronized analysis was conducted to accurately identify and distinguish true MS from false MS.

3.4 Data Acquisition

3.4.1 Vehicle-Based Data Acquisition and MS Scoring

In our experiments, our main focus was directly recording events related to both out-of-road (OOR) and on-road (OR) incidents using the driving simulator. The calculation for OOR was conducted through the interaction between the 'Mesh Collider' positioned on the lane boundary lines and the 'Wheel Collider' on the vehicle's wheels. The moment when the vehicle's wheel touched the boundary line was determined using the 'OnCollisionEnter' method. Similarly, the moment when the vehicle's wheel left the boundary line was identified using the 'OnCollisionExit' method. Contact with the boundary line indicated that the vehicle had moved out-of-road, while losing contact implied that the vehicle was on-road, as illustrated in Figure 3. 3.

Additionally, we intentionally avoided manual EEG-based scoring of MS episodes due to its inherent limitations. MS episodes are extremely brief, lasting from microseconds to 15 seconds [17][85]. In clinical settings, the lack of a standardized definition and an efficient scoring method often results in these short fragments being

overlooked [22]. Reliable assessment through visual inspection of EEG typically requires a minimum duration of 3 seconds, even though a significant portion of MS episodes

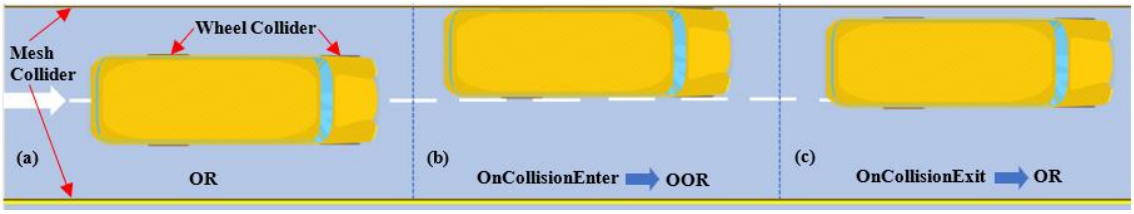

Figure 3. 3: OOR calculation is performed through the interaction of the 'Mesh Collider' placed on the boundary lines and the 'Wheel Collider' on the vehicle's wheels. (a) On-road episode (b) If the wheel collider contacts the mesh collider, this condition is called 'OnCollisionEnter' and is recorded as an OOR episode. (c) When the wheel collider loses contact with the mesh collider, this condition is called 'OnCollisionExit' and is recorded as an OR episode.

(40%) falls within the 1-3 second range [35][52]. Manual interpretation of such brief bursts of altered brain patterns during MS episodes is known to be highly challenging, susceptible to human error, and labor-intensive [17][22]. Another manual MS scoring approach involves combining EEG data, EOG data focusing on slow eye movements, and visual observations of eyelid closure exceeding 80% [17][22], but it fails to consider MS episodes with open eyes [50][53]. Our chosen method for MS scoring utilized psychomotor performance measures [49][51][86], which is a well-established approach for assessing MS, such as driving in a high-fidelity simulator. This method is based on scientific evidence indicating a significant correlation between MS episodes and subpar performance in simulated driving [17][46][47][87]. A few studies [46][47] have identified a moderate correlation between out-of-road (OOR) events and MS episodes. Therefore, we developed an objective MS scoring method based on OOR events recorded through the driving simulator. An MS episode was linked to an out-of-road event, labeled as an OOR (microsleep) event, when the vehicle's wheel contacted the lane boundary for a period of ≥ 1s. Conversely, a wakefulness episode was associated with an on-road (OR) event, labeled as an OR (wakefulness) event, when the vehicle's wheel disconnected from the lane boundary for ≥ 1s. We hypothesized that OOR (microsleep) events are primarily associated with MS episodes or patterns indicative of sleepiness, except for a few instances where fluctuations in driving performance, rather than sleepiness, may be a contributing factor [52][88]. This scoring approach can detect MS episodes lasting at least

1 second or longer, even when the person's eyes are open. As a result, the simulator recorded a total of 970 OOR (microsleep) and 1020 OR (wakefulness) events throughout the entire driving period, which were saved in a CSV file along with their corresponding timestamps. The collected data allowed us to analyze the frequency and duration of OOR (microsleep) events.

3.4.2 Physiological-Based Data Acquisition

The EEG signals from all six channels were stored in the European Data Format (EDF) using Noxturnal software, a specialized tool designed for recording, analyzing, and processing physiological data, specifically EEG signals [89]. In addition to the EEG data, time-related information such as the recording's start time and end time was also recorded.

3.5 Simultaneous Analysis of Vehicle-Based Signals and EEG Signals

Validation is a crucial component of studies utilizing simulators to assess driving performance [52][53]. In order to improve the accuracy and reliability of MS scoring using the DS, we integrated data from the DS, including OOR (microsleep) and OR (wakefulness) events, with synchronous EEG patterns to identify MS episodes. This approach was based on two established principles: (1) We focused on traditional frequency bands to validate the shift from the alpha to theta frequency band during MS episodes, as discussed in previous studies [22][35][90], and (2) We examined the complex interaction between fluctuations in sustained attention and the dynamic characteristics of the theta and alpha frequency bands, particularly in the frontal brain region, as documented in previous literature [82][91][92][93]. We hypothesized that the frontal brain region could accurately identify all MS episodes using the theta-to-alpha ratio as a reliable indicator. To test this hypothesis, we developed a custom program in MATLAB (R2022b) with specific features designed to detect associations between OOR (microsleep) events and brain patterns, thereby confirming the occurrence of MS episodes.

3.5.1 Filtering the EEG Signals

We implemented high-pass and low-pass filters as finite impulse response (FIR). The

high-pass filter had a cut-off frequency of 0.5 Hz, while the low-pass filter had a cut-off frequency of 30 Hz.

3.5.2 Loading and Processing CSV File

The start time and end time columns relevant to OOR (microsleep) and OR (wakefulness) events were extracted. Between two consecutive OOR (microsleep) events, there was an intervening OR (wakefulness) episode. During this OR (wakefulness) episode, the start time coincided with the end time of the preceding OOR (microsleep) event, and the end time aligned with the start time of the subsequent OOR (microsleep) event. The time intervals between the start and end times of OOR (microsleep) and OR (wakefulness) episodes were calculated and labeled as 'sub-lengths'.

3.5.3 *Splitting EEG Data into Epochs and Calculating PSD Using DWT*

In our study, we employed the discrete wavelet transform (DWT) using the 'db2' wavelet to analyze EEG data for each sub-length. DWT provided several technical advantages for EEG analysis. It offered precise time-frequency localization [94], enabling us to capture both transient [95] and sustained frequency changes essential for identifying specific EEG patterns related to brain activity. DWT facilitated efficient artifact removal by segregating artifacts based on frequency scales, thereby enhancing data quality [96]. Moreover, DWT played a crucial role in denoising EEG signals by decomposing them into different scales and selectively reducing or removing noise components [97], resulting in an improved signal-to-noise ratio. The capability of the 'db2' wavelet to capture transient and localized features was particularly beneficial in dynamic contexts [98]. We extracted approximations at level 3 and detail coefficients at levels 1, 2, and 3, representing the low and high-frequency components of the EEG signal. These coefficients were then categorized into frequency bands (beta, alpha, theta, delta), and power spectral density (PSD) was calculated for each band.

With the power computed for each band in every sub-length (OOR (microsleep) and OR (wakefulness) events), we proceeded to calculate the theta/alpha ratio for each event. Subsequently, we conducted a comparative analysis to determine whether the theta/alpha value for each OOR (microsleep) event was higher or lower than that of neighboring OR (wakefulness) episodes, as depicted in Figure 3. 4a. To visually present our findings in an intuitive manner, we generated a bar graph, as illustrated in Figure 3. 4b, effectively

showcasing the significant differences in theta/alpha ratios for OOR (microsleep) and OR (wakefulness) events. These steps ('3.5.1' to '3.5.3') were carried out to analyze the EEG data from all channels for a single participant. Additionally, we replicated these procedures to analyze data from all fifty subjects in our study.

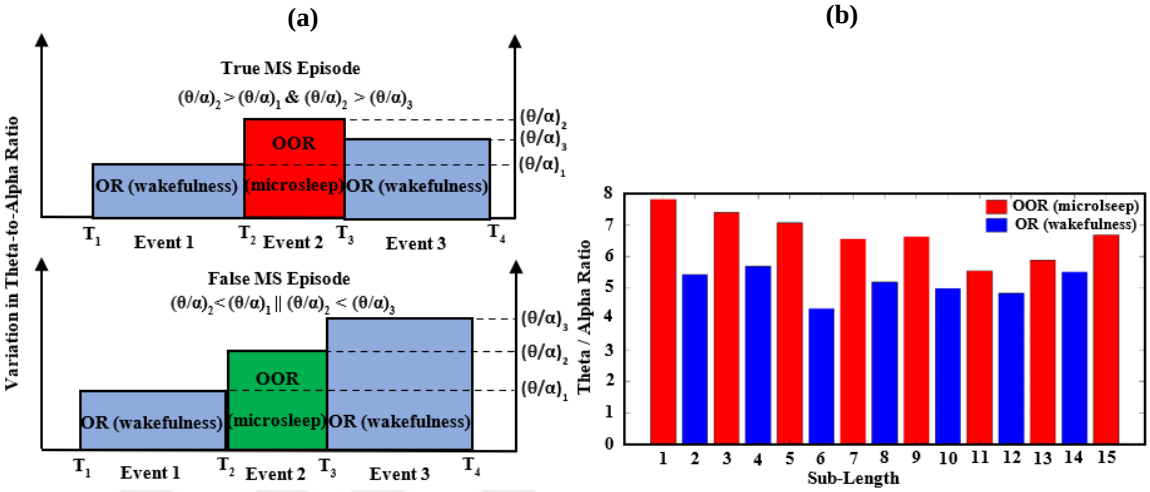

Figure 3. 4: (a) Comparative approach to identify true and false MS episodes by integrating driving attributes and brain patterns (b) Brain patterns of a participant where the theta/alpha ratio for all OOR (microsleep) events consistently exhibits higher values, while the theta/alpha ratio for all OR (wakefulness) episodes consistently shows lower values.

We classified an OOR (microsleep) event, where the brain exhibited specific variations in the theta-to-alpha ratio, including a decrease in theta-to-alpha ratio during the preceding OR (wakefulness) event, an increase in theta-to-alpha ratio during the OOR (microsleep) event, and then a decrease in theta-to-alpha ratio during the subsequent OR (wakefulness) event, as a true MS episode. Conversely, we categorized an OOR (microsleep) event, where the brain showed a decrease in theta-to-alpha ratio compared to the ratios of preceding or subsequent OR (wakefulness) events, as a false MS episode, as depicted in Figure 3. 4a. Based on the defined criteria, the algorithm identified and quantified instances where OOR events conformed to true or false MS episodes.

3.6 A Novel Way of Quantifying Maximum Drowsiness Level (MDL)

The maximum drowsiness level (MDL) signifies the peak point at which the driver's alertness significantly diminishes, potentially leading to impaired driving performance and an elevated risk of accidents [99]. We introduced an innovative approach to

quantifying the MDL experienced by drivers throughout their entire driving duration. Specifically, the MDL was determined by calculating the ratio between the maximum theta-to-alpha ratio observed during OOR (microsleep) events (indicating maximum drowsiness) and the minimum theta-to-alpha ratio observed during OR (wakefulness) episodes (indicating maximum alertness). The derived equation (3.1) allowed us to measure the extent to which drowsiness increases compared to alertness. A higher MDL value indicates a more pronounced difference between these two states.

$$\mathrm{MDL} = \frac{\text{Maximum } \left(\frac{\theta}{\alpha}\right) \text{ratio for OOR episodes}}{\text{Minimum } \left(\frac{\theta}{\alpha}\right) \text{ratio for OR episodes}} \tag{3.1}$$

Additionally, we performed a Pearson correlation analysis to investigate the connection between the frequency of MS episodes and the MDL. Our hypothesis suggested that a rise in MS frequency would align with a higher MDL. Through correlation analysis, our goal was to assess the magnitude and direction of the relationship between these variables.

3.7 Channel's Sensitivity in Identifying True MS Episodes

We hypothesized that the sensitivity of individual EEG channels would differ in accurately detecting true MS episodes, with the frontal brain region showing greater sensitivity compared to other regions. To test this hypothesis, we initially assessed the Identification Rate (IR) of true MS episodes for each channel among all participants. Following this, we computed the mean identification rates (MIRs) for each channel.

$$\mathrm{IR} = \frac{\text{True MS episodes}}{\text{Total OOR (microsleep)events}} \times 100 \tag{3.2}$$

$$\mathrm{MIR} = \frac{\text{Sum of IR of a channel across all subjects}}{\text{Total number of subjects}} \tag{3.3}$$

3.8 Temporal Features of True MS Episodes Among Drivers

The study involved several calculations, including determining the mean duration of MS episodes by averaging the durations of all true MS episodes, calculating the proportion of driving time spent in these episodes (referred to as 'cumulative time'), and measuring the latency to the first true MS episode for each driver. To assess the variability in these parameters, we computed the mean, standard deviation (SD), median, minimum, and maximum values, as well as the first quartile (Q1), third quartile (Q3), and

interquartile range (IQR) across all subjects. This analysis served as a baseline to identify any consistent trends in the temporal features of true MS episodes across the drivers.

3.9 Event Related Patterns (ERP) During OR and OOR Events

We hypothesized that significant differences exist in brain patterns during OR (wakefulness) and OOR (microsleep) events, as they are likely associated with distinct alert and drowsy states in the brain. To investigate this hypothesis, we conducted an analysis to quantify the variations in the theta-to-alpha ratio for both OOR (microsleep) and OR (wakefulness) events. Subsequently, we performed a Mann-Whitney U test to evaluate whether there were any significant differences in the median values of these variations between the two conditions.

Chapter 4:

METHODS FOR DROWSINESS DETECTION

4.1 Experimental Setup

The experimental setup used in this study is illustrated in Figure 4. 1. It comprises the XBUS PRO Driver Training Simulator (DTS) from ANGRUP Co., Istanbul, Turkey, the NOX-A1 EEG system by Nox Medical Inc. in Reykjavik, Iceland, and a 1080p camera as its core components. The DTS provided manual and automatic gearbox options and was outfitted with sensors that monitored throttle and brake usage, road deviations, steering anomalies, and possible accidents. Housed in a soundproof cabin, it provided a controlled environment with a constant temperature of 22°C for all participants and a 135-degree field of view. Using ANGRUP Software Technologies, the simulator replicated diverse road conditions such as straight stretches, circular tracks, curved paths, and low-traffic highways to simulate various driving scenarios. The EEG device, featuring 6

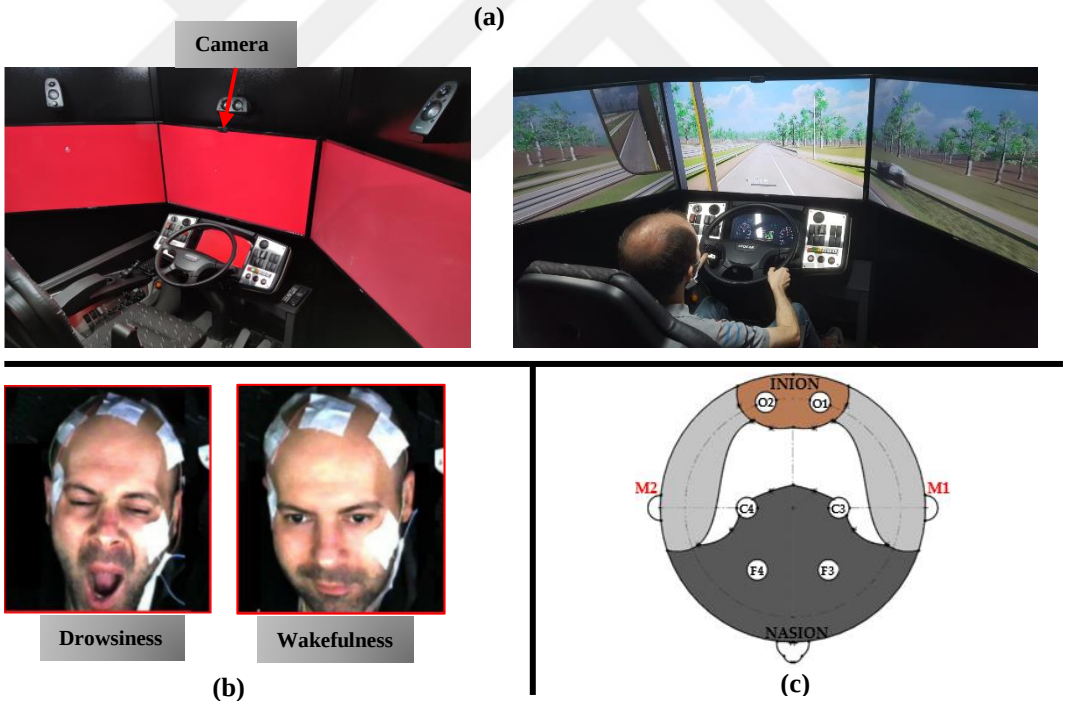

Figure 4. 1: (a) A high-fidelity driver training simulator comprising a driver cabin, camera system, voice communication setup, acceleration, and brake pedals, steering controls, offering both automatic and manual transmission modes, and providing diverse training scenarios [75]; (b) Facial video recording conducted by a 1080p camera mounted atop the middle view screen; (c) The International 10-20 system utilized for EEG electrode placement on the subject's scalp.

channels (Frontal: F4 & F3, Central: C4 & C3, Occipital: O1 & O2) and operated at a sampling rate of 200 Hz, capturing neural activity based on the standardized 10-20 electrode placement for consistent positioning [79]. Simultaneously, the dome camera recorded the driver's facial expressions at a rate of 30 frames per second.

4.2 Study Population and Subject Demographics

Previous research has indicated a notably higher prevalence of OSA among heavy vehicle professional drivers (42.2%) compared to the general population (5%) [100]. Moreover, the prevalence of OSA is higher in men (14%-50%) than in women (5%-23%) [101][102]. In our study, we used a bus driving simulator with professional drivers. It was conducted in Turkey, where bus driving is male dominated, resulting in the exclusive recruitment of male participants. Therefore, we enrolled fifty professional male drivers diagnosed with OSA based on their previous night's polysomnography results (apnea-hypopnea-index [AHI] ≥ 5.0 events/h) from the Sleep Laboratory for a simulator-assisted visual-based drowsiness detection [83]. Table 4. 1 provides the demographic details of the participants. The study protocol received approval from the Koç University Committee on Human Research (2020.292.IRB2.083; 19 June 2020), and written informed consent was obtained from all participants. Participants without acute illnesses were included, and they were advised to refrain from consuming caffeinated beverages, such as coffee and energy drinks, as well as other stimulants for 24 hours before the experiment [84].

Table 4. 1: Subjects vital statistics are presented. Each row displays the minimum-maximum (mean ± standard deviation) of a corresponding characteristic.

Parameters	**Value**
Sex	All are males
Body Mass Index (BMI)	23.5-41.9 (31.3 ± 4.4) kg / m^2
Age	32-68 (47.9 ± 7.6) year
Last night sleep hours	1-11 (6.3 ± 1.8) hour
Apnea-Hypopnea Index (AHI)	5-103.5 (29.8 ± 23.2) / hour
Oxygen Desaturation Index (ODI)	1.0-87.8 (24.4 ± 22.7) / hour

4.3 Experimental Design

Participants who met the eligibility criteria were scheduled for a simulated driving session between 08:00 AM and 10:00 AM, considering previous research that highlights increased risks during nighttime or early morning driving hours [103]. Prior to the experiment, a 10-minute training session familiarized drivers with vehicle controls and various driving scenarios, aiming to prepare them for the simulated tasks and enhance their performance. Additionally, the interior lights of the cabin were turned off to mimic real-world driving conditions. During the experiment, drivers engaged in a fifty-minute simulated driving session on a two-way highway, with maintained low traffic density and a maximum allowable speed of 62 mph (80 km/h). Figure 4. 2 illustrates the experimental design used in this study. Participants were equipped with a 6-channel EEG electrode setup to record their neural activity, and a frontal camera captured their facial expressions, with instructions to minimize head movements.

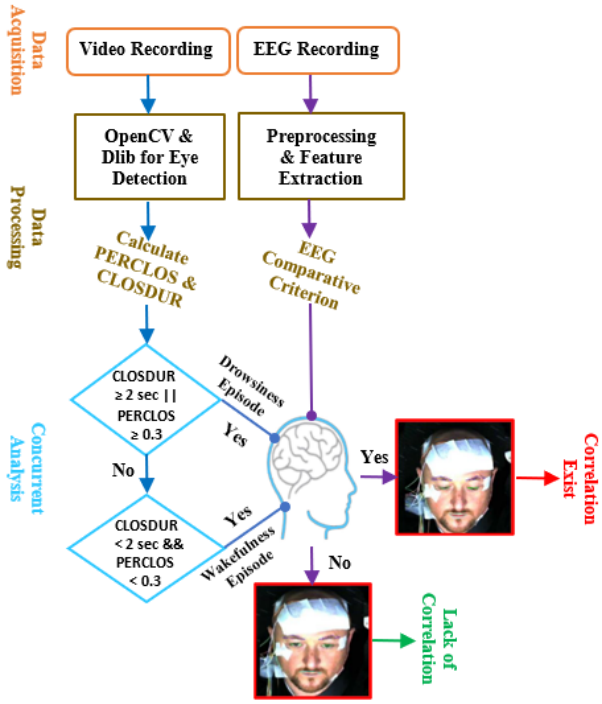

Figure 4. 2: The experiment design began with the acquisition of facial videos and EEG signals, followed by data processing and feature extraction. Subsequently, a concurrent analysis was conducted to validate visual-based scoring against EEG patterns, confirming onset of drowsiness.

4.4 *Data Acquisition*

4.4.1 Video-Based Data Acquisition and Drowsiness Scoring

In our study, we utilized visual-based scoring, an established technique for detecting drowsiness, by capturing facial video recordings of drivers engaged in simulated driving. Initially, we employed the Python-based OpenCV library to detect faces in the facial video recordings [104]. The detected faces then underwent a facial detection procedure using the Dlib library, which allowed us to estimate landmark positions on each detected face [105]. The Dlib library's pretrained face landmark detector provided coordinates for 68 points, covering regions around the eyes, eyebrows, mouth, nose, and chin, as shown in Figure 4. 3a . Subsequently, we computed the eye aspect ratio (EAR) by calculating the Euclidean distance between the identified eye landmarks (refer to Figure 4. 3b), as outlined in Equation (4.1).

$$\mathrm{EAR} = \frac{|\mathrm{P}_2 - \mathrm{P}_6| + |\mathrm{P}_3 - P_5|}{2|\mathrm{P}_1 - \mathrm{P}_4|} \tag{4.1}$$

(a) **(b)**

Figure 4. 3: (a) 68 facial landmark points provided by Dlib library (b) Open and closed eyes with detected landmark points. These points around the eye are used to calculate EAR.

The EAR value typically maintains stability when the eye is open but drops to zero during a blink. Past studies have proposed different EAR thresholds, suggesting that values below 0.28 [106], 0.25 [107], 0.20 [108], 0.18 [109], and 0.16 [110] indicate eye blinking or closure. However, utilizing a fixed threshold value across different

individuals, varied lighting conditions, and eyewear presence does not yield precise EAR calculations. Momentary facial expressions like yawning or smiling, as well as head rotations, underscore the necessity for an adaptive threshold value that accommodates diverse individuals and situational factors. The adaptive threshold incorporated a median filter to attenuate abrupt changes in EAR values, effectively reducing noise. Next, employing a moving average filter ensured smoother transitions in EAR values over time, mitigating the impact of environmental variations. Subsequently, the threshold value underwent dynamic readjustment by subtracting a constant value (0.04) following the application of the median filter (of length 17) and moving average filter (of length 5). The filter parameters were determined experimentally. This iterative process continuously refined the threshold based on updated EAR values, significantly improving the precision and adaptability of our technique. Figure 4. 4 illustrates the steps of the adaptive threshold method and compares it with the fixed threshold (EAR = 0.2, suggested by [108]). It highlights the successful detection of eye blinks marked with green ellipses by the adaptive threshold method, contrasting instances missed by the fixed threshold.

After applying adaptive thresholding to detect eye blinks during the driving session, we calculated two metrics: PERCLOS, which indicates the ratio of frames with closed eyes to the total frames with both closed and open eyes, and CLOSDUR, which measures the duration of eye closure. By following established criteria for defining drowsiness (PERCLOS $\geq$ 0.3 or CLOSDUR $\geq$ 2 sec) and wakefulness (PERCLOS $<$ 0.3 and CLOSDUR $<$ 2 sec) episodes [41], we identified a total of 927 instances encompassing both drowsiness (n=453) and wakefulness (n=474) events throughout the entire driving session. These instances were saved in a CSV file along with their respective timestamps.

4.4.2 Physiological Signal-Based Data Acquisition

EEG signals from all six channels were recorded in the European Data Format (EDF) using the Noxturnal software, a specialized tool designed for recording, analyzing, and processing various physiological data types, including EEG signals [89]. Along with EEG data, temporal information including the start time and end time of the recording was also noted.

4.5 Concurrent Analysis of Visual-Based Scoring with EEG Patterns

While visual-based scoring is acknowledged as a valid method for detecting

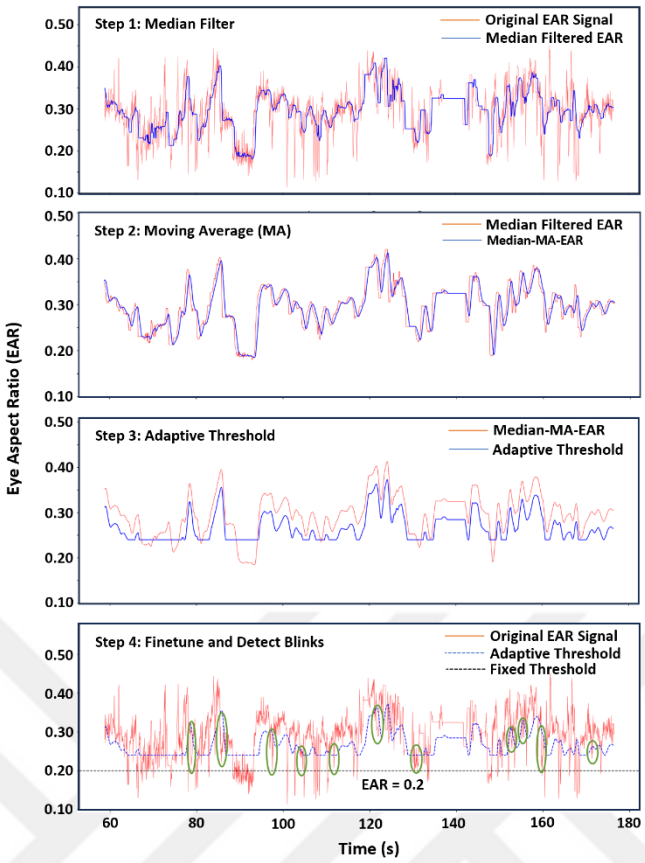

Figure 4. 4: Steps of blink detection using eye-aspect-ratio: Following the extraction of EAR values from video frames, step 1 applies a median filter to reduce sudden and fast variations, noticeable when comparing the original signal and its median-filtered version. Step 2 smoothens the signal and reduces short-term swings with a moving average filter, as demonstrated by the Median-MA-EAR signal. Step 3 employs an adaptive threshold to enhance accuracy and make the signal condition adaptive. Step 4 finetunes the parameters and selects consecutive signals falling below the threshold to identify blinks (green ellipses).

drowsiness [40][41], the inherent challenges in accurately computing PERCLOS underscore the importance of validating this technique using physiology-based signals. To enhance the accuracy and reliability of visual-based scoring, we combined data from drowsiness and wakefulness events, obtained through visual-based scoring, with synchronized EEG patterns. This integration aimed to establish a meaningful correlation between these two metrics. To achieve this objective, we developed a customized MATLAB (R2022b) program with specific features designed to identify associations between visual-based scoring and EEG patterns.

4.5.1 Filtering the EEG Signals

We designed finite impulse response (FIR) filters, both high-pass and low-pass, with an order of 25 using the equiripple design method to balance filter complexity and achieve sharpness in frequency response transition regions [77]. This design aimed at optimal attenuation in the stopband while preserving passband characteristics essential for EEG analysis. The high-pass filter, with a cutoff frequency of 1 Hz, effectively attenuates low-frequency artifacts (0.17-0.24 Hz range) commonly caused by eye blinks [111]. Conversely, the low-pass filter, with a cutoff frequency of 30 Hz, was intended to exclude high-frequency noise and potential artifacts originating from electromyogram (EMG) signals [112].

4.5.2 Loading and Processing CSV File

The relevant columns containing the start and end times for visual-based drowsiness and wakefulness episodes were extracted for analysis. Between two consecutive drowsiness events, a wakefulness episode occurred, with the start time of the wakefulness event aligning with the end time of the previous drowsiness episode, and the end time of the wakefulness event aligning with the start time of the next drowsiness episode.

4.5.3 Splitting EEG Data into Epochs and Computing PSD using DWT

In our study, we employed an established discrete wavelet transform (DWT) with the 'db2' wavelet to analyze EEG data per visual-based episode. DWT is suitable for analyzing non-stationary signals like EEG due to its optimal resolution in both time and frequency domains, allowing precise localization of time-frequency components critical for identifying specific EEG patterns related to brain activity [94][95]. It also aids artifact removal by segregating artifacts based on frequency scales, enhancing data quality, and denoising EEG signals by decomposing them into different scales and selectively reducing noise components, resulting in an improved signal-to-noise ratio [96][97] [75]. We chose the 'db2' wavelet function for its established effectiveness in EEG analysis, particularly valuable in dynamic contexts [98][113]. A study on EEG signal classification showed that the Daubechies wavelets, specifically the db2 wavelet, achieved 97.2% accuracy, surpassing coeif4, sym10, db1, and db6 [114]. At level 3 decomposition, we extracted approximation and detail coefficients, representing unique frequency components within the EEG signal. These coefficients were separated into beta (15-30)

Hz, alpha (7.5-15) Hz , theta (4-7.5) Hz, and delta (1-4) Hz frequency bands, as detailed in Figure 4. 5.

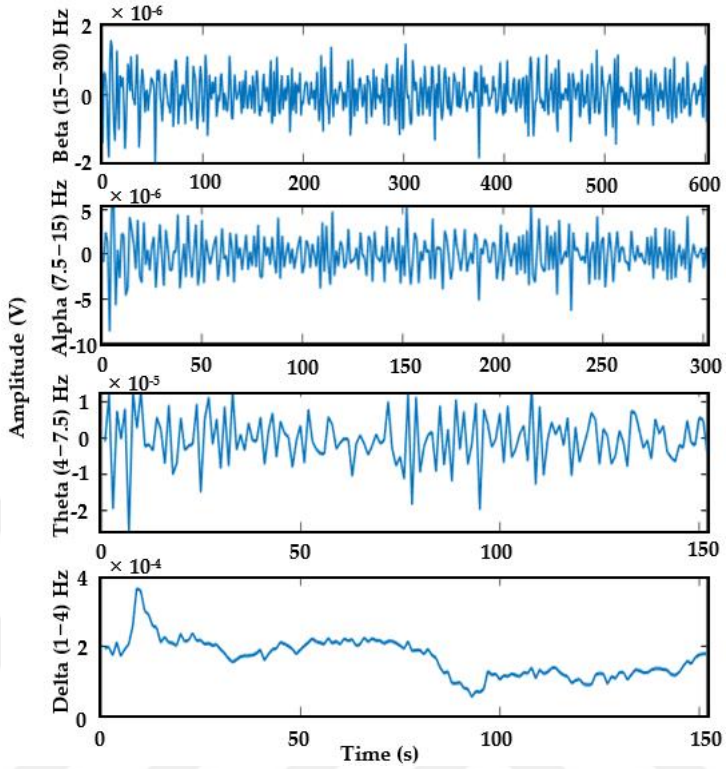

Figure 4. 5: Detail and approximation coefficients associated with their respective frequency bands (beta, alpha, theta, and delta) obtained through the implementation of DWT.

Power spectral density (PSD) was computed for each band (PSD alpha, PSD theta, and PSD delta) using MATLAB's 'bandpower' function to measure the signal's power within these specific ranges, including their respective ratios (theta to alpha, delta to alpha, and delta to theta), for each episode identified through visual-based scoring. We hypothesized that during the transition from wakefulness to drowsiness, PSD alpha decreases, while PSD theta, PSD delta, and theta to alpha, delta to alpha, delta to theta ratios exhibit opposite trends. Additionally, we also calculated spectral entropy (SE), spectral spread (SS), spectral centroid (SC), and spectral rolloff (SRO) using the following computations:

SE quantifies the level of complexity or randomness present in the power spectrum of an EEG signal. A high SE value indicates a signal with high complexity and unpredictability, often associated with a wakeful state. In contrast, a low SE value suggests a more predictable and periodic signal, commonly observed during drowsiness or sleep states [115][116].

$$H = -\sum_{f=0}^{L-1} n_f . log_2(n_f) \tag{4.2}$$

SE is calculated by first normalizing the spectral energy across all frequency bands. This normalization involves dividing the energy in each frequency band by the total energy across all bands. Following normalization, SE is determined by summing the product of the normalized energy in each band and the logarithm (typically base 2) of that normalized energy. This summation is performed across all frequency bands involved in the analysis [117].

SS quantifies the variability in the distribution of spectral energy within an EEG signal. It assesses the breadth of the power spectrum and reveals how energy is distributed around the spectral centroid, providing insight into the 'sharpness' or 'flatness' of the spectrum. We suggested that higher SS values are associated with drowsiness episodes, while lower values are indicative of wakefulness episodes.

$$S_i = \sqrt{\frac{\sum_{k=1}^{WfL}(k - C_i)^2 X_i(k)}{\sum_{k=1}^{WfL} X_i(k)}} \tag{4.3}$$

SS is computed as the square root of the weighted variance of the squared differences between each frequency and the spectral centroid. It represents the standard deviation of the frequency components around the spectral centroid. This computation requires the value of C_i, the spectral centroid, to be determined first [117].

SC represents the 'center of mass' of the power spectrum of an EEG signal. It corresponds to the average frequency of the power spectrum, weighted by the amplitude of each frequency component. We hypothesized that elevated SC values are associated with wakefulness episodes, whereas lower values tend to indicate drowsiness.

$$C_i = \frac{\sum_{k=1}^{WfL} kX_i(k)}{\sum_{k=1}^{WfL} X_i(k)} \tag{4.4}$$

The value of the spectral centroid, C_i, for the ith frame is computed by taking the sum of each frequency multiplied by its corresponding amplitude, divided by the sum of all amplitudes. where k represents the frequency index, $X_i(k)$ is the amplitude at frequency k, and WfL is the windowed frame length over which the computation is performed [117].

SRO is the frequency below which a defined percentage (typically 85% to 95%) of the total spectral energy is contained. It is a measure used to describe the skewness of the

power spectrum. We proposed that higher SRO values are linked with wakefulness, whereas lower values suggest drowsiness.

$$\sum_{k=1}^{m} X_i(k) = C \sum_{k=1}^{WfL} X_i(k) \tag{4.5}$$

SRO for the ith frame is calculated by identifying the frequency bin, m, such that the cumulative sum of amplitudes up to frequency bin m is equal to a percentage C of the total sum of amplitudes, where C is the rolloff percentage (e.g., 0.9 for 90%) [117].

The objective of computing of the aforementioned ten EEG features was to pinpoint the most robust correlation between EEG patterns and visual-based scoring by examining these features. To achieve this, we established ten separate comparative criteria for each feature. These criteria aimed to identify whether a feature's value during a drowsiness event exceeded or fell below neighboring wakefulness episodes, as detailed in Table 4. *2*.

This analytical process, encompassing steps labeled '2.5.1' to '2.5.3', was executed on EEG data across all channels for each participant. This methodology was then replicated across all fifty subjects within our study cohort. We categorized visual-based drowsiness and wakefulness episodes based on adherence to these established criteria. Episodes meeting the criteria were classified as indicating a correlation, while those not conforming were deemed indicative of a lack of correlation, as depicted in Figure 4. 6. Employing these predefined criteria, the algorithm evaluated Spearman's correlation between episodes from visual-based scoring and instances where individual EEG features matched with these episodes across all channels. Spearman's correlation evaluates the relationship between two variables using a monotonic function, suiting our data that doesn't meet the normality assumption [118]. Figure 4. 7 shows the concurrent analysis of visual-based scoring and EEG patterns (theta-to-alpha ratio) captured by channel F4. Notably, episodes 5, 16, 17, 24, 25, and 26 did not meet the established criteria, thus indicating a lack of correlation.

4.6 EEG Channels and Brain Regions Sensitivity in Correlating Visual Scoring with EEG Patterns

Our hypothesis aimed to evaluate the sensitivity of individual EEG channels and brain regions in establishing correlations between visual-based scoring and EEG patterns, characterized by ten distinct features, across fifty drivers. The objective was to identify the feature that demonstrates the strongest correlation and determine which specific EEG

Table 4. 2: Ten criteria illustrate distinct EEG features for correlation with visual-based scoring, where 'i' represents drowsiness episodes, and ‘i-1’ and ‘i+1’ denote the preceding and subsequent wakefulness episodes derived from visual-based scoring.

EEG Feature	Criterion for Correlation
Theta-to-alpha ratio	theta_alpha_ratio(i) > theta_alpha_ratio(i-1) && theta_alpha_ratio(i+1)
Delta-to-alpha-ratio	delta_alpha_ratio(i) > delta_alpha_ratio(i-1) && delta_alpha_ratio(i+1)
Delta-to-theta-ratio	delta_theta_ratio(i) > delta_theta_ratio(i-1) && delta_theta_ratio(i+1)
PSD Alpha	PSD_alpha(i) < PSD_alpha(i-1) && PSD_alpha(i+1)
PSD Theta	PSD_theta(i) > PSD_theta (i-1) && PSD_theta(i+1)
PSD Delta	PSD_delta(i) > PSD_delta (i-1) && PSD_delta(i+1)
Spectral-Entropy	PSD_entropy(i) < PSD_entropy (i-1) && PSD_entropy(i+1)
Spectral Spread	PSD_spread(i) > PSD_spread (i-1) && PSD_spread(i+1)
Spectral Centroid	PSD_centroid(i) < PSD_centroid (i-1) && PSD_centroid(i+1)
Spectral Rolloff	PSD_rolloff(i) < PSD_rolloff (i-1) && PSD_rolloff(i+1)

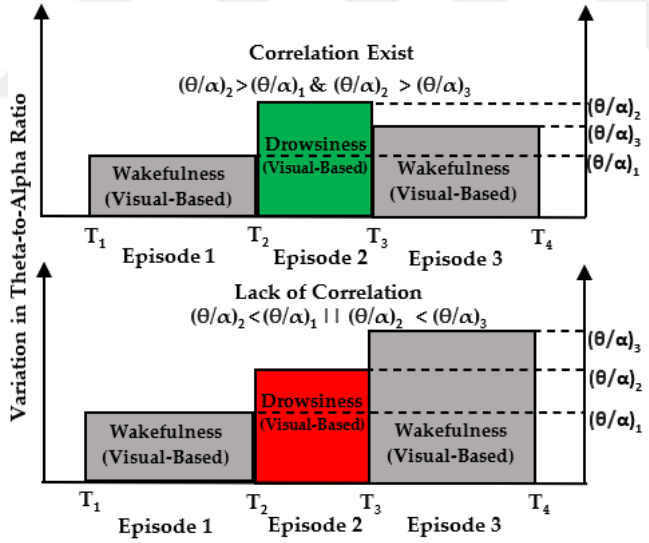

Figure 4. 6: A comparative approach used to determine the presence of correlation by combining episodes from visual-based scoring with EEG patterns.

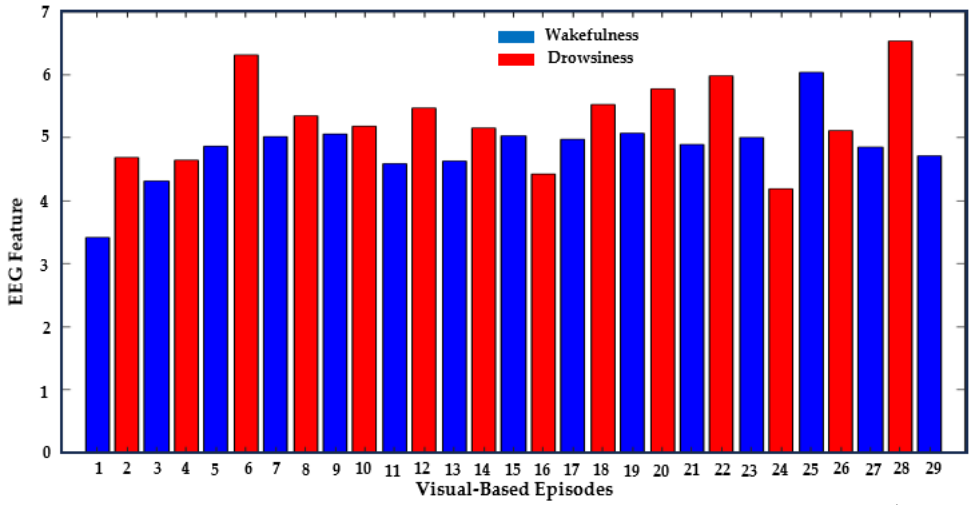

Figure 4. 7: This figure presents a concurrent analysis of a participant (ID:1055). Blue and red bars represent neighboring wakefulness and drowsiness episodes determined by visual-based scoring throughout the entire driving period, with the length of the bar indicating the corresponding EEG patterns (theta-to-alpha ratio). In this instance, visual-based scoring recorded 15 wakefulness and 14 drowsiness events (total: 29 episodes). Comparative criterion for theta-to-alpha ratio reveals that EEG patterns correlate with 23 episodes of visual-based scoring, demonstrating F4-channel sensitivity of 79.3% (23/29)×100).

channel or brain region contributes most significantly to this correlation. To achieve this, we first calculated the average sensitivity (see Equation (4.7)) of individual EEG channels in detecting this correlation across a cohort of fifty drivers based on each feature's comparative criterion. Subsequently, we assessed the average combined sensitivity of paired EEG channels (F4/F3, C4/C3, and O1/O2), followed by the average combined sensitivity of all EEG channels for each feature, using the same cohort and criterion (see Equation (4.9)).

$$\text{Sensitivity of a Channel} = \frac{\text{Episodes showing correlation}}{\text{Total Number of episodes}} \times 100 \tag{4.6}$$

$$\text{Average Sensitivity} = \frac{\text{Sum of sensitivty of a channel across all subjects}}{\text{Total number of subjects}} \tag{4.7}$$

$$\text{Comb. Sens.} = \left[1 - \frac{\text{Events not correlated by merging channels}}{\text{Total number of episodes}}\right] \times 100 \tag{4.8}$$

$$\text{Average Comb. Sens.} = \frac{\text{Sum of combine sensitivity across all subjects}}{\text{Total number of subjects}} \tag{4.9}$$

Chapter 5:
OPTIMIZING EEG CHANNELS AND FEATURES

5.1 EEG Channels and EEG Features Optimization

In our former study [75], we assessed the sensitivity of individual EEG channels and different brain regions (frontal, central, occipital), as well as the collective sensitivity of all six channels, focusing on the theta/alpha ratio. 'Sensitivity' refers to a channel's effectiveness in capturing variations in the EEG feature corresponding to wakefulness and drowsiness states identified through vehicle-based scoring (on-road and off-road episodes) using a comparative criterion. This criterion compares the theta/alpha ratio of a drowsiness episode with the preceding and subsequent theta/alpha ratios of wakefulness episodes to validate potential drowsiness episodes. Our analysis revealed varying sensitivities across different channels, with channel F4 showing particularly high sensitivity. Combining channels according to brain regions notably amplified sensitivity, especially in the frontal region. Additionally, integrating all six channels significantly increased sensitivity. This exploration concluded that sensitivity increases with the addition of more channels, as depicted in Figure 5. 1.

In our subsequent study [76], we focused on ten different EEG features instead of a single feature. This approach allowed us to explore whether varying the types of features across different channels would yield increased sensitivity in capturing variations related to drowsy and wakeful episodes derived from visual-based scoring. Our analysis examined the unique sensitivities of individual EEG features across each channel, highlighting notable instances of heightened sensitivity in channels F4 and O2. This demonstrated significant amplification in sensitivity when channels were aggregated by brain region. Furthermore, integrating all six channels enhanced sensitivity across all features. This analysis confirmed that sensitivity increases with channel aggregation across all features, as explained in Figure 5. 1.

We hypothesized that pairing various EEG features, rather than combining different channels, could achieve coverage with individual channels (F4 or O2) comparable to or better than using all six channels. This approach could reduce hardware and computational requirements while maintaining efficacy. Additionally, we not only correlated visual-based scoring with EEG patterns but also employed a classification

technique, which could potentially benefit real-time drowsiness detection. Figure 5. 2 provides an overview of the complete algorithm used to validate this hypothesis.

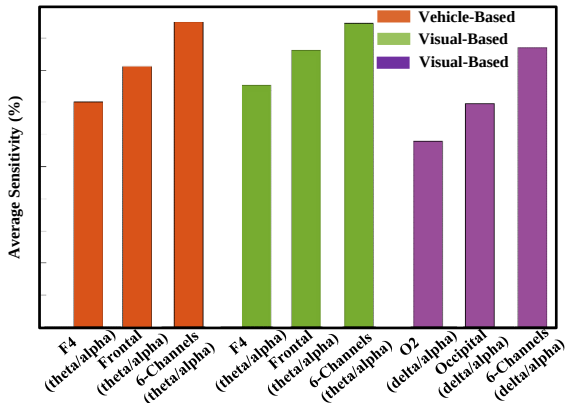

Figure 5. 1: The red and green bars illustrate that the average sensitivity of matching EEG patterns (theta/alpha ratio) with vehicle-based scoring or visual-based scoring increases with the addition of EEG channels. Additionally, the green and purple bars depict that the average sensitivity of EEG features (theta/alpha and delta/alpha) varies based on the individual EEG channels and the number of EEG channels.

5.1.1 Normalization of EEG Features

The EEG features extracted for each epoch underwent normalization to standardize them onto a comparable scale (ranging from 0 to 1), as achieved by the equation (1). This normalization process aimed to mitigate the substantial discrepancies in raw values observed across different features for each epoch.

$$Normalized\ Feature_{(i)} = \frac{featureData_{(i)} - \ min.featureData_{(i)}}{max.featureData_{(i)} - \ min.featureData_{(i)}} \qquad (5.1)$$

The variable 'featureData$_{(i)}$' represents the raw data for the feature 'i'. The functions min. and max. are employed to determine the minimum and maximum values of 'featureData$_{(i)}$', respectively.

5.1.2 Computing Subject-Specific and Feature-Specific Thresholds

In our work, we opted for thresholding over a comparative criterion to classify between wakeful and drowsy states for each feature. This approach may enable real-time classification, facilitating efficient differentiation between the two states. Determining the optimal subject-specific and feature-specific threshold presented a

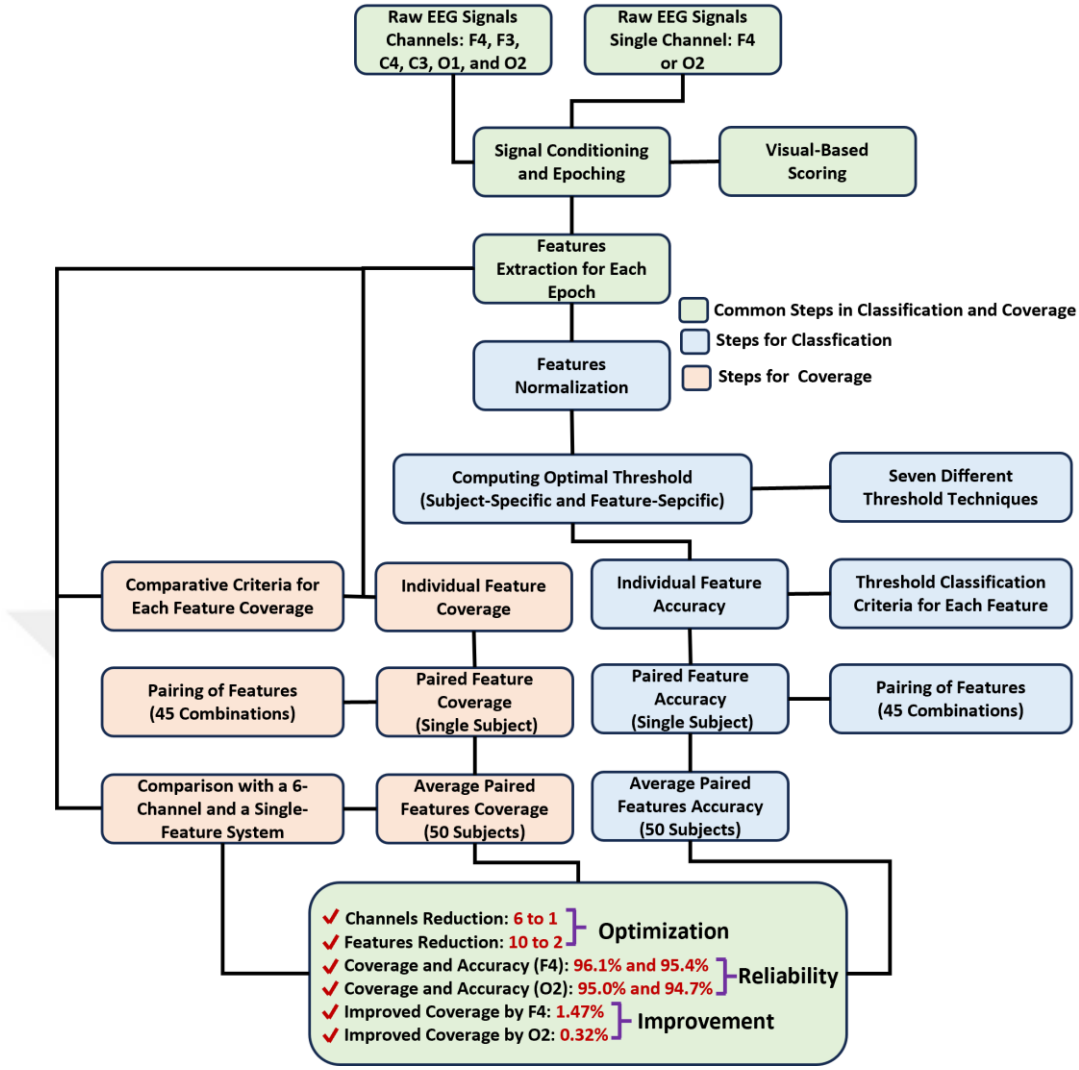

Figure 5. 2: This figure illustrates the algorithm employed to optimize both EEG channels (from 6 to 1) and EEG features (from 10 to 2), with the aim of achieving at least the same average coverage as that achieved with 6 EEG channels. Additionally, it focuses on the accuracy of EEG channels (F4 and O2) in identifying drowsiness based on subject-specific and feature-specific thresholding.

significant challenge in our methodology, aiming for consistent threshold calculation across fifty subjects and ten features. The objective was to select a threshold technique that could effectively differentiate all wakeful and drowsy episodes, correlating accurately with visual-based scoring. We experimented with various thresholding techniques to identify the most suitable threshold for each feature and subject, ensuring uniformity in threshold calculation across different EEG features and subjects. The computations of thresholds were performed according to equations 5.2 through 5.22, systematically replicated for all features and subjects.

- **Threshold based on Arithmetic Mean (AM)**

$$AM_{wakeful\ (i)} = \text{mean (normalizedFeatues}_i\ (visual\_scoring), 1) \quad (5.2)$$

$$AM_{drowsy(i)} = \text{mean (normalizedFeatues}_i\ (\sim visual\_scoring), 1) \quad (5.3)$$

$$Threshold_{AM\ (i)} = \frac{AM_{wakeful\ (i)} + AM_{drowsy(i)}}{2} \quad (5.4)$$

- **Threshold based on Standard Deviation (Std)**

$$Std_{wakeful\ (i)} = std\ (normalizedFeatues_i\ (visual\_scoring), 1) \quad (5.5)$$

$$Std_{drowsy(i)} = std\ (normalizedFeatues_i\ (\sim visual\_scoring), 1) \quad (5.6)$$

$$Threshold_{Std\ (i)} = \frac{Std_{wakeful\ (i)} + Std_{drowsy(i)}}{2} \quad (5.7)$$

- **Threshold based on Median (M)**

$$M_{wakeful\ (i)} = median\ (normalizedFeatues_i\ (visual\_scoring), 1) \quad (5.8)$$

$$M_{drowsy(i)} = median\ (normalizedFeatues_i\ (\sim visual\_scoring), 1) \quad (5.9)$$

$$Threshold_{M\ (i)} = \frac{M_{wakeful\ (i)} + M_{drowsy\ (i)}}{2} \quad (5.10)$$

- **Threshold based on Trimean (TM)**

$$TM_{wakeful\ (i)} = \frac{Q1_{wakeful\ (i)} + 2 \times M_{wakeful\ (i)} + Q3_{wakeful\ (i)}}{4} \quad (5.11)$$

$$TM_{drowsy\ (i)} = \frac{Q1_{drowsy\ (i)} + 2 \times M_{drowsy\ (i)} + Q3_{drowsy\ (i)}}{4} \quad (5.12)$$

$$Threshold_{TM\ (i)} = \frac{TM_{wakeful\ (i)} + TM_{drowsy\ (i)}}{2} \quad (5.13)$$

- **Threshold based on Median Absolute Deviation (MAD)**

$$MAD_{wakeful\ (i)} = \text{mad (normalizedFeatues}_i\ (visual\_scoring), 1) \quad (5.14)$$

$$MAD_{drowsy(i)} = \text{mad (normalizedFeatues}_i\ (\sim visual\_scoring), 1) \quad (5.15)$$

$$Threshold_{MAD\ (i)} = \frac{MAD_{wakeful\ (i)} + MAD_{drowsy(i)}}{2} \quad (5.16)$$

- **Threshold based on Inter Quartile Range (IQR)**

$$IQR_{wakeful(i)} = Q3_{wakeful\ (i)} - Q1_{wakeful(i)} \quad (5.17)$$

$$IQR_{drowsy(i)} = Q3_{drowsy\ (i)} - Q1_{drowsy(i)} \quad (5.18)$$

$$Threshold_{IQR\ (i)} = \frac{IQR_{wakeful(i)} + IQR_{drowsy(i)}}{2} \quad (5.19)$$

- **Threshold based on Robust Scaling (RS)**

$$RS_{wakeful\ (i)} = \frac{M_{wakeful(i)} - Q1_{wakeful(i)}}{IQR_{wakeful}} \quad (5.20)$$

$$RS_{drowsy\ (i)} = \frac{M_{drowsy(i)} - \ Q1_{drowsy(i)}}{IQR_{drowsy}} \tag{5.21}$$

$$Threshold_{RS\ (i)} = \frac{RS_{wakeful\ (i)} + \ RS_{drowsy\ (i)}}{2} \tag{5.22}$$

5.1.3 Classification Criteria for Each Feature Based on Threshold

'$Feature_i$' epochs were classified based on whether the '$normalizedFeatures_i$' value is above or below a calculated '$threshold_i$'. The decision to classify an epoch as indicating drowsy (or wakeful) was determined by the specific criteria set for each feature, as explained in Table 5. 1.

Table 5. 1: This table illustrates the individual criterion for each feature to classify drowsy or wakeful episodes based on thresholding technique.

EEG Feature	**Criterion for Classification Based on Threshold**
theta/alpha-ratio	Here indice 'i' shows a feature 'theta/alpha ratio' if $NormalizedFeatures_i > Threshold_i$ Epoch is classified as drowsy else $NormalizedFeatures_i < Threshold_i$ Epoch is classified as wakeful
delta/alpha ratio	Criterion similar to that of 'theta/alpha ratio'
delta/theta ratio	Criterion similar to that of 'theta/alpha ratio'
PSD alpha	Here indice 'i' shows a feature 'PSD alpha' if $NormalizedFeatures_i < Threshold_i$ Epoch is classified as drowsy else $NormalizedFeatures_i > Threshold_i$ Epoch is classified as wakeful
PSD theta	Criterion similar to that of 'theta/alpha ratio'
PSD delta	Criterion similar to that of 'theta/alpha ratio'
Spectral entropy	Criterion similar to that of 'PSD alpha'
Spectral spread	Criterion similar to that of 'theta/alpha ratio'
Spectral centroid	Criterion similar to that of 'PSD alpha'
Spectral rolloff	Criterion similar to that of 'PSD alpha'

5.1.4 Combined Coverage and Accuracy of Paired Features

We utilized a logical OR operation to combine the individual classification accuracy of paired features (totaling 45 combinations) for each subject. This procedure evaluated whether either feature effectively categorizes the epoch's state as drowsy or wakeful, consistent with visual-based scoring. Additionally, we assessed the collective coverage of each combination using comparative criteria (see Table 5. 2), as illustrated by the following MATLAB code lines. This step aimed to elucidate the relative resemblance between the collective coverage based on comparative criteria and the combined accuracy achieved through threshold technique, ensuring the reliability of our methodology.

- combinedClassification=(classifiedEpisodes1==visual_scoring)|(classifiedEpisodes2 == visual_scoring)
- combinedAccuracy = mean(combinedClassification) × 100
- combinationCoverage = feature_matrix(:, i) | feature_matrix(:, j)
- combinedCoverage = mean(combinationCoverage) × 100

'feature_matrix' serves as a repository for recording matched instances (marked as 1) and non-matched instances (marked as 0) of features against visual-based scoring, utilizing individual comparative criterion.

5.1.5 Average Combined Accuracy of Each Paired Features Across Fifty Subjects

After computing the combined accuracy and coverage of all possible paired features for a single subject, we replicated steps from sr. # 5.1.1 to 5.1.4 across fifty subjects to determine the average combined accuracy and coverage. This process is summarized by the following equations. We also identified the top three pairs that most effectively classified drowsy and wakeful episodes, across fifty subjects.

$$Average\ Combined\ Accuracy = \text{mean (combinedAccuracy)} \quad (5.23)$$

$$Average\ Combined\ Coverage = \text{mean (combinedCoverage)} \quad (5.24)$$

Table 5. 2: This table illustrates the individual criterion for each feature to match visual-based scoring. Here, epoch(i), epoch(i – 1), and epoch (i + 1) correspond drowsy, preceding, and subsequent wakeful episodes derived from visual-based scoring.

EEG Feature	**Novel Comparative Criterion: Comparing Drowsy Episode Value with the Values of Adjacent wakeful events**
theta/alpha-ratio	Here indice 'i' shows drowsy episode derived from visual-based scoring If theta_alpha_ratio(i) > theta_alpha_ratio(i - 1) && theta_alpha_ratio(i) > theta_alpha_ratio(i + 1) Epoch(i), epoch(i – 1), and epoch(i + 1) match with visual-based scoring elseif theta_alpha_ratio(i) > theta_alpha_ratio(i - 1) && theta_alpha_ratio(i) <= theta_alpha_ratio(i + 1) Epoch(i + 1) doesn't match with visual-based scoring elseif theta_alpha_ratio(i) <= theta_alpha_ratio(i - 1) && theta_alpha_ratio(i) > theta_alpha_ratio(i + 1) Epoch(i - 1) doesn't match with visual-based scoring else Epoch(i), epoch(i – 1), and epoch(i + 1) don't match with visual-based scoring
delta/alpha-ratio	Criterion similar to that of 'theta/alpha ratio'
delta/theta-ratio	Criterion similar to that of 'theta/alpha ratio'
Psd alpha	Here indice 'i' shows drowsy episode derived from visual-based scoring If PSD_alpha(i) < PSD_alpha(i - 1) && PSD_alpha(i) < PSD_alpha(i + 1) Epoch(i), epoch(i – 1), and epoch(i + 1) match with visual-based scoring elseif PSD_alpha(i) < PSD_alpha(i - 1) && PSD_alpha(i) >= PSD_alpha(i + 1) Epoch(i + 1) doesn't match with visual-based scoring elseif PSD_alpha(i) >= PSD_alpha(i - 1) && PSD_alpha(i) < PSD_alpha(i + 1) Epoch(i - 1) doesn't match with visual-based scoring else Epoch(i), epoch(i – 1), and epoch(i + 1) don't match with visual-based scoring
Psd theta	Criterion similar to that of 'theta/alpha ratio'
Psd delta	Criterion similar to that of 'theta/alpha ratio'
Spectral entropy	Criterion similar to that of 'PSD alpha'
Spectral spread	Criterion similar to that of 'theta/alpha ratio'
Spectral spread	Criterion similar to that of 'PSD alpha'
Spectral rolloff	Criterion similar to that of 'PSD alpha'

Chapter 6:
RESULTS FOR MICROSLEEP DETECTION

6.1 A Significant Correlation Between OOR (microsleep) Events and True MS Episodes

The concurrent analysis successfully established a correlation between synchronized EEG patterns and driving behaviors. It revealed that during nearly all OOR (microsleep) events, there was a consistent increase in the theta-to-alpha ratio compared to the ratios observed in preceding and subsequent OR (wakefulness) events. This finding aligns well with the first established concept we utilized. Initially, our focus was on individual EEG channels (F4, F3, C4, C3, O1, and O2) to visualize brain patterns during OOR (microsleep) and OR (wakefulness) events. We observed that individual channels F4 and F3 correctly identified 677 and 606 out of 970 OOR (microsleep) events as true MS episodes, respectively. When combined, channels F4 and F3 collectively identified 791 out of 970 OOR (microsleep) events as true MS episodes, as detailed in Table 6. 1. To determine the collective identification of true MS episodes across paired channels (F4 and F3, C4 and C3, O1 and O2), we selected the higher value (true MS episodes) between the individual channels within each paired channel across all subjects. Among the combinations explored, the frontal channels (F4 and F3) exhibited the strongest correlation with OOR (microsleep) events and true MS episodes. This outcome significantly validates the reliability of the second concept we utilized.

It is noteworthy that when we expanded our analysis to encompass all channels used in the study, our methodology demonstrated an even higher correlation, accurately identifying 923 out of 970 OOR (microsleep) events as true MS episodes, achieving an impressive matching rate of 95.15%. This indicates that 47 out of 970 OOR (microsleep) events may have been influenced by variations in driving performance rather than solely attributed to sleepiness. Considering our initial aim of quantifying true MS episodes using a minimal number of EEG channels or a specific brain region, we subsequently narrowed our focus to the frontal channels. This enabled us to calculate the maximum drowsiness level (MDL), analyze the temporal details of true MS episodes, and examine the variance in theta-to-alpha ratio between OR (wakefulness) and OOR (microsleep) episodes across all subjects. Figure 6. 1 visually presents the results of the simultaneous analysis for three subjects, with a particular focus on the frontal brain region.

Table 6. 1: This table represents the results of the simultaneous analysis, indicating a higher matching of OOR (microsleep) events as True MS episodes by the frontal brain region compared to other brain regions.

Brain Region	OOR (microsleep) Events	True MS Episodes
Frontal	970	791
Central		543
Occipital		459
Combining all regions		923

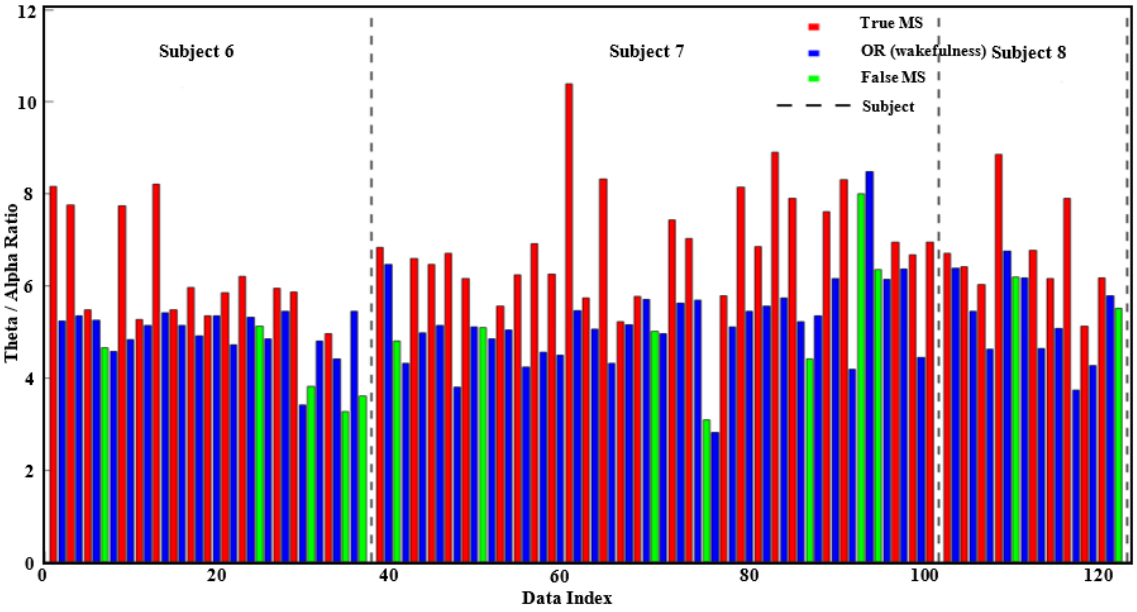

Figure 6. 1: The simultaneous analysis highlights the instances where OOR (microsleep) events correctly identified as True MS episodes (depicted by red bars), and those where OOR (microsleep) events do not correspond to true MS episodes, recognized as false MS episodes (depicted by green bars). This differentiation is based on the brain patterns or theta-to-alpha ratio, particularly focusing on the frontal brain region.

6.2 Quantification of Maximum Drowsiness Level and its Strong Positive Correlation with Density of True MS

The mean of the maximum drowsiness level (MDL) was determined to be 2.5518 ± 1.0873, with minimum and maximum values of 1.2500 and 5.3000, respectively, across all drivers. Detailed statistical parameters of MDL are provided in Table 6. 2. Pearson

correlation analysis unveiled a statistically significant correlation ($r = 0.8913$, $p < 0.001$) between the MDL experienced by each driver throughout the entire driving period and the density of MS episodes, as depicted in Figure 6. 2a . The coefficient of determination (R-squared) value of 0.7943 indicates that approximately 79.43% of the variance in MDL can be elucidated by the linear regression model using the density of MS as the predictor variable.

Table 6. 2: This table provides detailed statistical parameters of maximum drowsiness level (MDL), variance in theta-to-alpha ratio during OOR (microsleep) and OR (wakefulness) events, MS duration, cumulative time of true MS episodes and latency to first true MS episode across all drivers.

Feature	**Mean**	**SD**	**Min.**	**Max.**	**Median**	**Q1**	**Q3**	**IQR**	**Confidence Interval**
Maximum Drowsiness Level	2.5518	1.0873	1.2500	5.3000	2.2700	1.6800	3.1500	1.4700	[1.2575, 5.1500]
Variance in OOR	1.4339	1.0616	0.0044	4.2684	1.1316	0.6066	2.0190	0.7484	[0.0151, 4.2077]
Variance in OR	0.5531	0.4805	0.0000	1.8030	0.3987	0.1864	0.9550	0.7686	[0.0000, 1.5710]
MS duration (s)	1.3330 to 11.5000	0.5774 to 14.8492	1.00	48.00	1.0000 to 11.5000	1.0000 to 7.0000	1.7500 to 22.0000	0.7500 to 21.0000	-
Cumulative time of MS (%)	3.0547	2.3971	0.1000	9.6667	2.6000	1.1333	4.0667	2.9333	[0.1250, 9.2917]
Latency to First MS (min.)	12.8467	9.5468	2.5000	43.28	9.5167	6.2500	16.8167	10.5667	[3.2875, 42.7083]

6.3 Higher Sensitivity of Frontal Channels in Identifying True MS Episodes

We evaluated the mean identification rate (MIR) of each EEG channel in detecting true MS episodes across all drivers. Figure 6. 2(b-c) depicts the MIR for individual and combined channels, respectively. Notably, individual channels F4 and F3 exhibited higher MIRs of 70.16% and 65.98%, respectively, compared to other channels. To assess the efficacy of combining channels in enhancing identification rates, we explored all feasible channel pairs. For each pair, the data-driven code selected the higher IR value from their individual IR values across all subjects. By calculating the mean of these higher IR values, we obtained the combined mean of IR (CMIR) value for that specific channel pair. Remarkably, the channel pair F4/F3 demonstrated a higher CMIR value of 83.70% compared to other channel combinations.

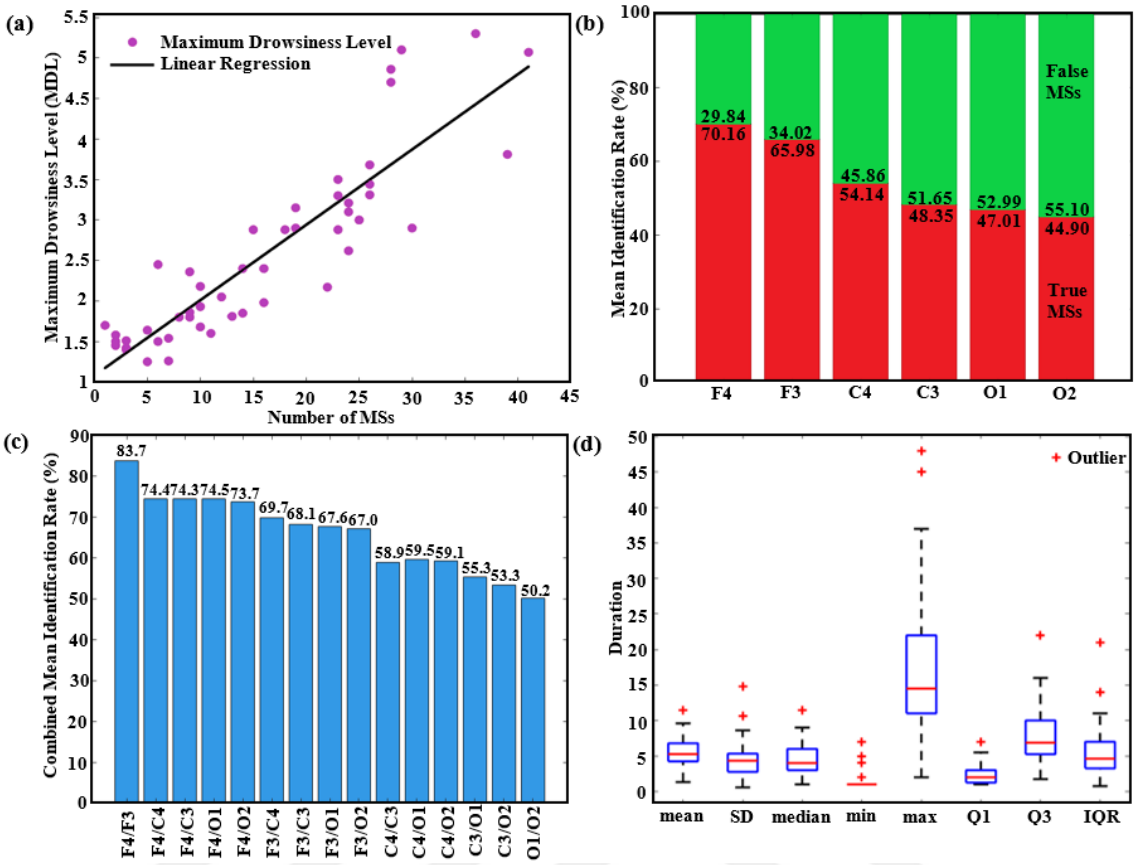

Figure 6. 2: (a) Positive linear relationship in between density of true MS episodes and maximum drowsiness level (b) Mean identification rate of each channel shows that channel F4 is more sensitive in identifying true MS episodes across all channels (c) Combined mean identification rate by combining two channels shows that frontal channels pair (F3 and F4) is more sensitive in identifying true MS episodes (d) Substantial variations in mean, standard deviation (SD), median, minimum value (min), maximum value (max), first quartile (Q1), third quartile (Q3) and inter quartile range (IQR) of MS durations among the drivers.

6.4 Temporal Features of True MS Episodes Across the Drivers

The mean duration of MS episodes, cumulative time of all true MS episodes, and latency to the first true MS episode for each driver were calculated. (Refer to Table 6. 2 for a detailed statistical analysis of the temporal features of true MS episodes across all drivers). The analysis revealed no significant correlation between the density of true MS episodes and their mean duration ($p > 0.05$) among all drivers. However, a strong and

significant correlation was identified between the frequency of true MS episodes and their cumulative time ($r = 0.9075$, $p < 0.001$), as well as between cumulative time and the maximum drowsiness level across all subjects ($r = 0.8816$, $p < 0.001$). Additionally, a moderate and statistically significant negative correlation was observed between the frequency of OOR (microsleep) events and the latency to the first true MS episode across all subjects ($r = -0.30$, $p < 0.05$). Figure 6. 2d demonstrates the substantial variations in the statistical parameters, highlighting the significant diversity in the duration of MS episodes among drivers. It's noteworthy that the observed range of MS durations spanned from 1 second to 48 seconds among drivers. Moreover, the duration of 95% of all MS episodes fell within the range of 1 to 15 seconds, as depicted in Figure 6. 3a.

6.5 Event Related Patterns (EPR) in the Brain During OR (wakefulness) and OOR (microsleep) Events

We conducted an analysis to determine the variances in the theta-to-alpha ratio associated with OOR (microsleep) and OR (wakefulness) events among a sample of 50 drivers, as detailed in Table 6. 2. Figure 6. 3b visually represents the variance in brain patterns observed during these events. The mean variance in the theta-to-alpha ratio for OR (wakefulness) events was calculated to be 0.5531 ± 0.4805, indicating a relatively consistent theta-to-alpha ratio across the drivers during wakefulness. Conversely, the mean variance in the theta-to-alpha ratio for OOR (microsleep) events was determined to be 1.4339 ± 1.0616, pointing towards significant fluctuations in brain activity among all drivers during microsleep episodes. We employed the Mann-Whitney U test, suitable for non-normally distributed and non-paired data (refer to Table 6. 3), to assess the effect of episode type on the variance in the theta-to-alpha ratio, revealing a statistically significant effect ($p<0.001$). This outcome suggests substantial differences in brain patterns between OR (wakefulness) and OOR (microsleep) events.

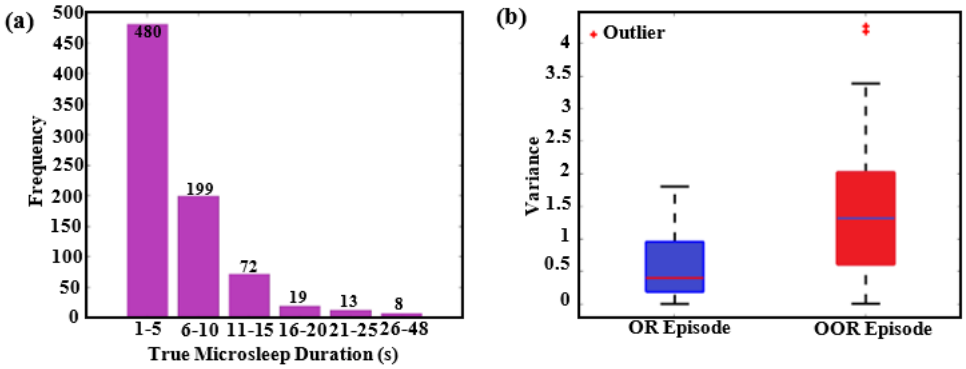

Figure 6. 3: (a) The frequency for different intervals of true MS duration clearly shows that 95% of the duration falls within the range of 1 to 15 seconds (b) The error bar plot clearly shows that brain has significantly different patterns during OR (wakefulness) and OOR (microsleep) events based on theta to alpha variance.

Table 6. 3: p-value in the table shows that the brain has distinct different patterns during OR (wakefulness) and OOR (microsleep) events.

Parameter	**Value**
p-value	$p < 0.001$
Mann-Whitney U Statistic	1
Effect Size (Cohen's d)	-1.069

Chapter 7:
RESULTS FOR DROWSINESS DETECTION

7.1 Significant Correlation Between Visual-Based Scoring and EEG Patterns Across all Channels

The concurrent analysis effectively validated visual-based scoring by establishing direct correlations between synchronous EEG patterns, characterized by ten specific features, and episodes of drowsiness and wakefulness derived from it. Out of 927 visual-based scoring episodes analyzed, 878 showed matching EEG patterns across all channels, thereby significantly enhancing the reliability of drowsiness detection (refer to Table 7. 1). While all EEG features displayed statistically significant correlations, as detailed in Table 7. 2, the theta-to-alpha ratio demonstrated a stronger association ($r = 0.9971$, $p < 0.001$) with visual-based scoring compared to the other analyzed features. Moreover, we noted variations in this correlation by adjusting the number of channels, their positions around the head, and specific EEG features, as illustrated in Figure 7. 1.

Table 7. 1: This table presents the number of episodes where visual-based scoring aligns with EEG patterns (theta-to-alpha ratio) across all channels, analyzed concurrently.

Episodes	Visual-Based Scoring	Matched Episodes
Drowsiness	453	427 (94.3%)
Wakefulness	474	451 (95.1%)
Total Episodes	927	878 (94.7%)

Table 7. 2: Spearman's correlations calculated between episodes derived from visual-based scoring and instances where individual EEG features matched with these episodes across all six channels. This analysis encompassed a cohort of fifty subjects.

EEG Feature	Pearson Correlation
Theta-to-alpha ratio	$r = 0.9942$, $p < 0.001$
Delta-to-alpha-ratio	$r = 0.9768$, $p < 0.001$
Delta-to-theta-ratio	$r = 0.9826$, $p < 0.001$
PSD-Alpha	$r = 0.9757$, $p < 0.001$
PSD-Theta	$r = 0.9633$, $p < 0.001$

PSD-Delta	r = 0.9777, p < 0.001
Spectral-Entropy	r = 0.9268, p < 0.001
Spectral Spread	r = 0.9816, p < 0.001
Spectral-Centroid	r = 0.9843, p < 0.001
Spectral-Rolloff	r = 0.9826, p < 0.001

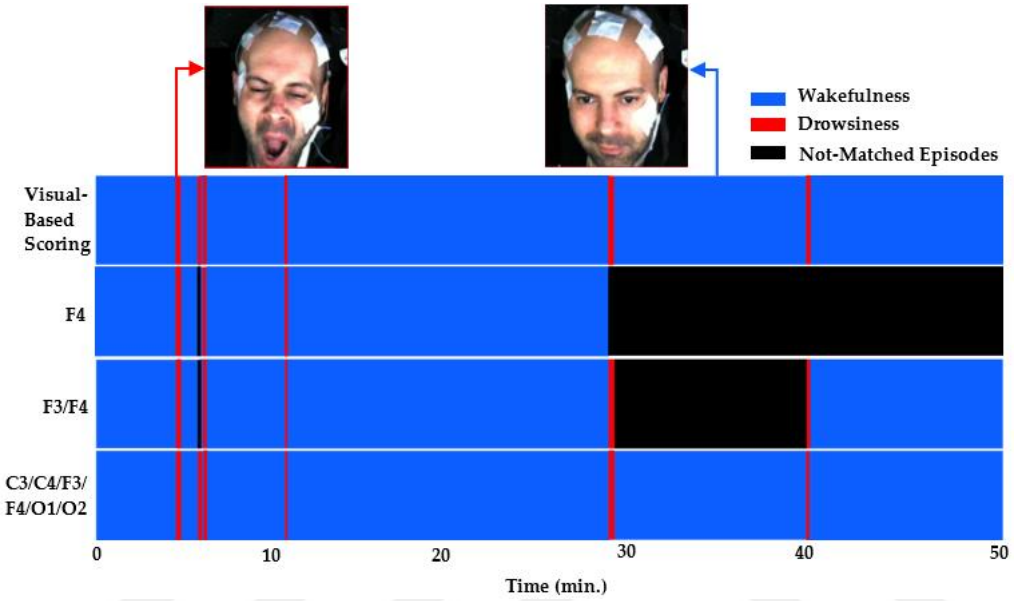

Figure 7. 1: This figure depicts the matching between visual-based scoring and EEG patterns (subject ID:1025), showcasing variations with the number of channels. The top row presents visual-based scoring, encompassing six drowsiness and seven wakefulness events. Subsequent rows demonstrate the matching of these episodes with EEG patterns based on different channels: the second row with channel F4, the third by combining channels F3 and F4, and the last using all channels. Notably, all visual-based episodes corresponded with EEG patterns in the combined channel setup.

7.2 Enhanced Sensitivity of F4 and O2 Channels, and Frontal and Occipital Brain Regions in Correlating Visual-Based Scoring with EEG Patterns

We conducted an assessment to determine the average sensitivity of individual EEG channels and specific brain regions in establishing correlations between visual-based scoring episodes and ten distinct EEG features across a group of fifty drivers. Notably, channel F4 demonstrated higher average sensitivity (75.4%) in correlating visual-based scoring with the EEG feature of theta-to-alpha ratio, as depicted in Figure 7. 2. Table 7. 3 outlines the channels with heightened sensitivity compared to others for each EEG

feature. Interestingly, no central channel (C3 or C4) exhibited higher sensitivity for any EEG feature. Similarly, the frontal brain region exhibited higher average combined sensitivity (86.4%) in illustrating the correlation between visual-based scoring episodes and the theta-to-alpha ratio compared to other brain regions, as illustrated in Figure 7. 3. Table 7. 4 provides details on the brain regions with increased sensitivity compared to others for each EEG feature. An in-depth analysis across all channels revealed that the theta-to-alpha ratio displayed the highest average combined sensitivity (94.7%) in correlation with visual-based scoring, as depicted in Figure 7. 4. Additionally, other metrics such as spectral spread (87.8%), spectral centroid (87.4%), delta-to-alpha ratio (87.2%), delta-to-theta ratio (86.7%), and spectral rolloff (86.4%) also exhibited notable sensitivity. Figure 7. 5 portrays the variability in sensitivity across channel F4, the frontal brain region, and all channels among the fifty subjects considering the theta-to-alpha ratio.

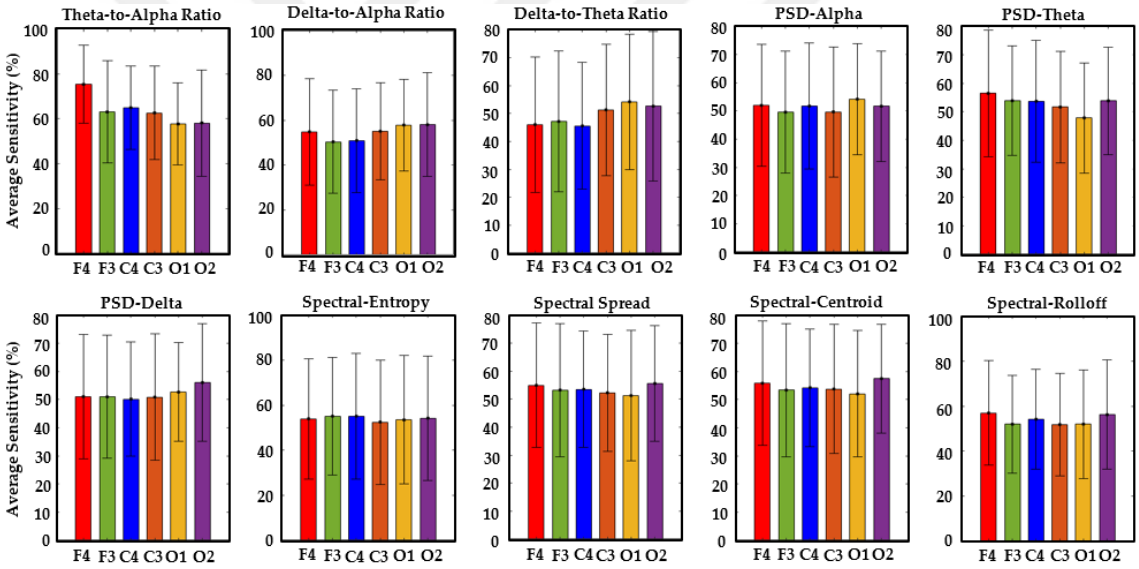

Figure 7. 2: This figure shows the average sensitivity of individual EEG channels in detecting correlations between episodes of visual-based scoring and ten specific EEG features across fifty drivers. The theta-to-alpha ratio emerged as a crucial feature for effectively correlating EEG patterns with visual-based scoring and channels F4 and O2 maintained consistent superiority across most EEG features.

Table 7. 3: This table illustrates the heightened average sensitivity of a single EEG channel for each EEG feature. Additionally, it presents the trend depicting how each EEG feature varies with increasing drowsiness.

EEG Feature	EEG Channel	Average Sensitivity	Trend
Theta-to-alpha ratio	F4	75.4%	↑
Delta-to-alpha-ratio	O2	58.0%	↑
Delta-to-theta-ratio	O1	54.2%	↑
PSD-Alpha	O1	54.2%	↓
PSD-Theta	F4	56.5%	↑
PSD-Delta	O2	56.1%	↑
Spectral-Entropy	F3	55.1%	↓
Spectral Spread	O2	55.6%	↑
Spectral-Centroid	O2	57.5%	↓
Spectral-Rolloff	F4	57.0%	↓

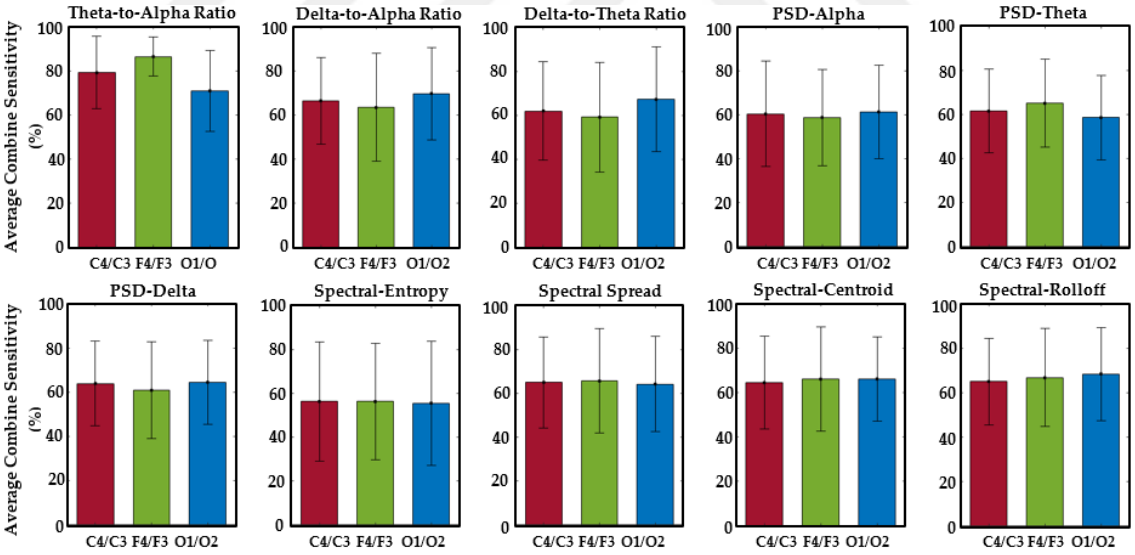

Figure 7. 3: This figure illustrates the average combine sensitivity of paired EEG-channels across brain regions in detecting correlations between episodes of visual-based scoring and ten specific EEG features in a cohort of fifty drivers. Notably, the frontal and occipital regions sustained consistent supremacy across most EEG features in establishing this correlation. The central brain region did not exhibit supremacy for any of the features.

Table 7. 4: This table illustrates the heightened average combined sensitivity of a brain region for each EEG feature.

EEG Feature	Brain Region	Average Combine Sensitivity
Theta-to-alpha ratio	Frontal	86.4%
Delta-to-alpha-ratio	Occipital	69.7%
Delta-to-theta-ratio	Occipital	67.3%
PSD-Alpha	Occipital	61.3%
PSD-Theta	Frontal	65.1%
PSD-Delta	Occipital	64.1%
Spectral-Entropy	Frontal	56.3%
Spectral Spread	Frontal	65.6%
Spectral-Centroid	Occipital	66.1%
Spectral-Rolloff	Occipital	68.4%

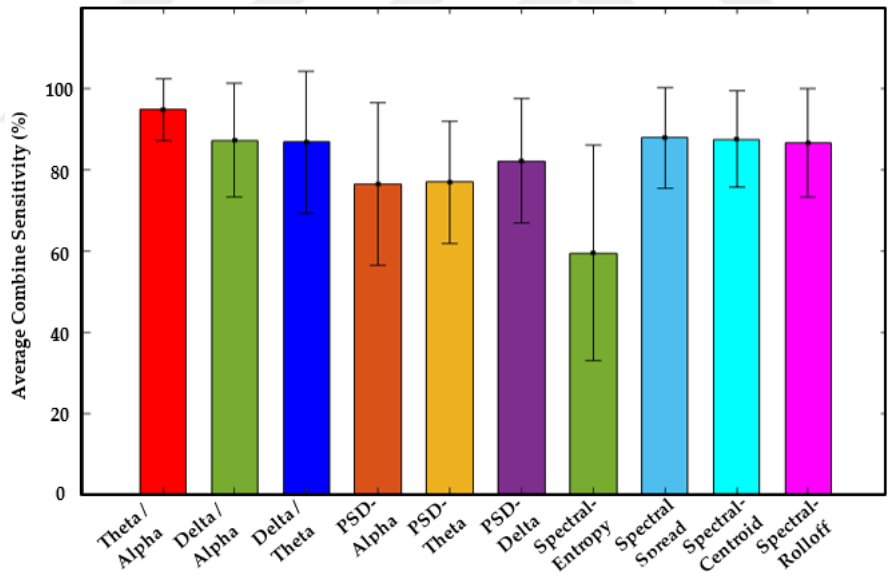

Figure 7. 4: This figure illustrates the average combine sensitivity of all EEG-channels (F3/F4/C3/C4/O1/O2) in detecting correlations between episodes of visual-based scoring and ten specific EEG features across a cohort of fifty drivers. Notably, all of the features except spectral entropy demonstrated average combine sensitivity more than 75%.

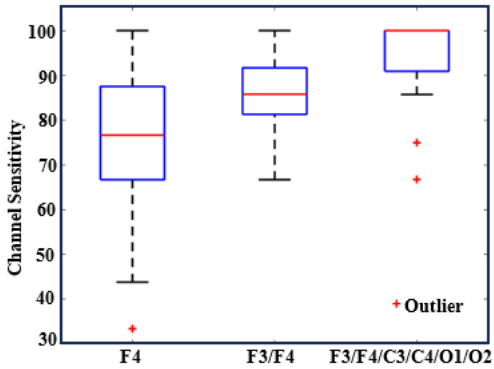

Figure 7. 5: This figure illustrates the decrease in variability of channel sensitivity with an increasing number of channels.

Chapter 8:

RESULTS FOR OPTIMIZING EEG CHANNELS

8.1 Enhanced Average Combined Coverage and Accuracy of Paired Features for Channels F4 and O2

We calculated thresholds for each feature and noted that their values vary not only across features within a subject but also across different subjects. We determined the mean combined coverage using comparative criteria and the average combined accuracy employing thresholding across 45 paired features, encompassing fifty subjects. Among the plethora of combinations, we present in Figure 8. 1 and Figure 8. 2 the top three combinations for channels F4 and O2 exhibiting not only heightened mean combined coverage but also elevated average combined accuracy. Furthermore, to elucidate the impact of feature combination, we assessed the average individual coverage and accuracy, illustrating the enhancements achieved by optimal features pairing. For channel F4, this improvement is evident in the combination of PSD alpha and PSD theta, where the mean combined coverage and accuracy reach 96.1% and 95.4%, respectively, representing a significant enhancement over their individual counterparts, which are 52.0% and 49.5%, respectively, for PSD alpha, and 56.5% and 54.7%, respectively, for PSD theta. For channel O2, we noted a similar improvement in the same combination of PSD alpha and PSD theta, with the mean combined coverage and accuracy reaching 95.0% and 94.7%, respectively. This indicates a notable improvement over their corresponding individual values, which are 51.7% and 49.6%, respectively, for PSD alpha, and 53.9% and 53.8%, respectively, for PSD delta. It is notable that across all three combinations and their individual counterparts, the mean coverages and accuracies display a remarkable similarity, with the mean coverage for each combination and its counterparts slightly higher. This consistent trend persists across all possible feature combinations and their corresponding individual values, thereby bolstering the reliability of our methodology. Furthermore, Channel F4 exhibited slightly higher values for mean combined coverage and average combined accuracy compared to Channel O2.

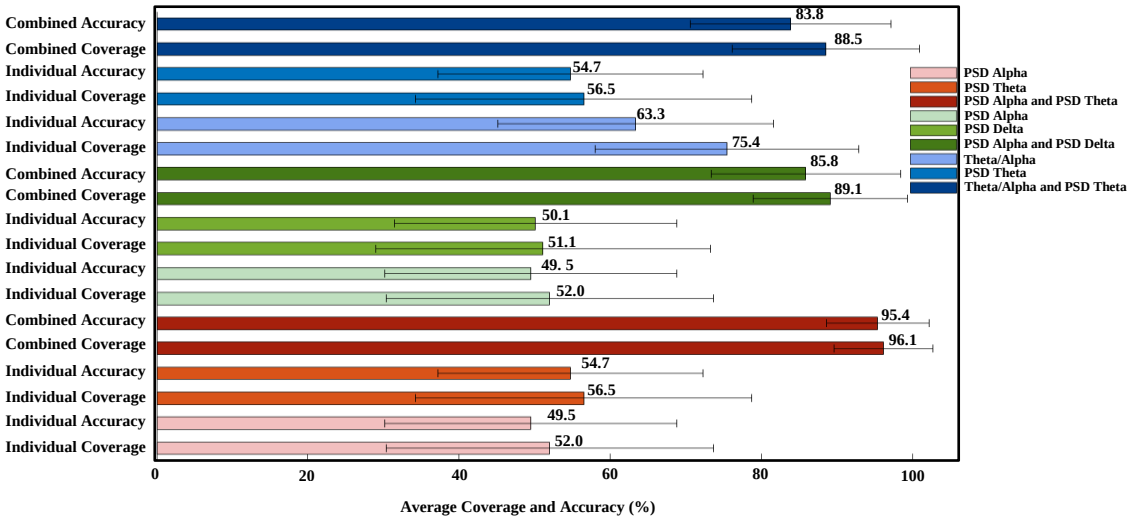

Figure 8. 1: This figure illustrates the mean combined accuracy, determined by the median threshold, and the average combined coverage, assessed against comparative criteria, for the top three paired features along with their individual values for channel F4 across fifty subjects. The combination of PSD alpha and PSD theta emerges as the optimal choice, followed by the combinations of PSD alpha and PSD delta, and theta/alpha ratio and PSD theta.

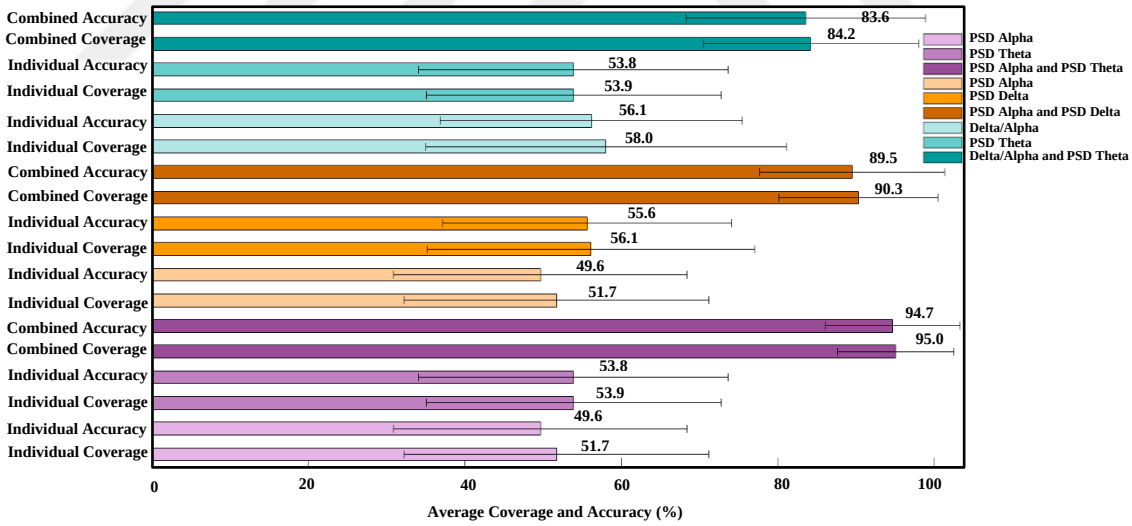

Figure 8. 2: This figure illustrates the mean combined accuracy, determined by the median threshold, and the average combined coverage, assessed against comparative criteria, for the top three paired features along with their individual values for channel O2 across fifty subjects. The paired feature combination of PSD alpha and PSD theta emerges as the optimum choice, followed by the combinations of PSD alpha and PSD delta, and delta/alpha ratio and PSD theta.

8.2 EEG Channels Optimization Based on Paired Features Comparable to Multichannel System

We also assessed that by integrating EEG features (PSD alpha and PSD theta) for channels F4 and O2, the average combined coverage increased to 96.1% for channel F4 and 95.0% for channel O2, compared to the mean combined coverage of 94.7% obtained by considering all six channels with one feature (theta/alpha ratio), as depicted in Figure 8. 3. This integration optimized channel utilization, reducing hardware requirements from 6 EEG electrodes to 1 EEG electrode for the same purpose, with slightly greater efficacy (1.47% in case of channel F4 and 0.32% in case of channel O2).

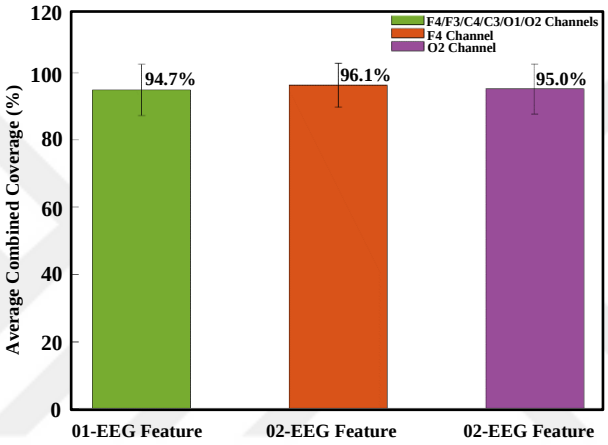

Figure 8. 3: This figure clearly shows that the average combined coverage of individual channels F4 and O2, achieved by combining two optimal features out of ten, exceeds the average combined coverage obtained by integrating six channels using one feature.

8.3 Variation in Average Combined Accuracy by Altering Thresholding Techniques

We also evaluated variations in average combined accuracy and their individual counterparts with changes in the threshold computing technique. We determined heightened average combined accuracy (95.4%) for PSD alpha and PSD theta by employing threshold calculation based on the median compared to other techniques, as illustrated in Figure 8. 4.

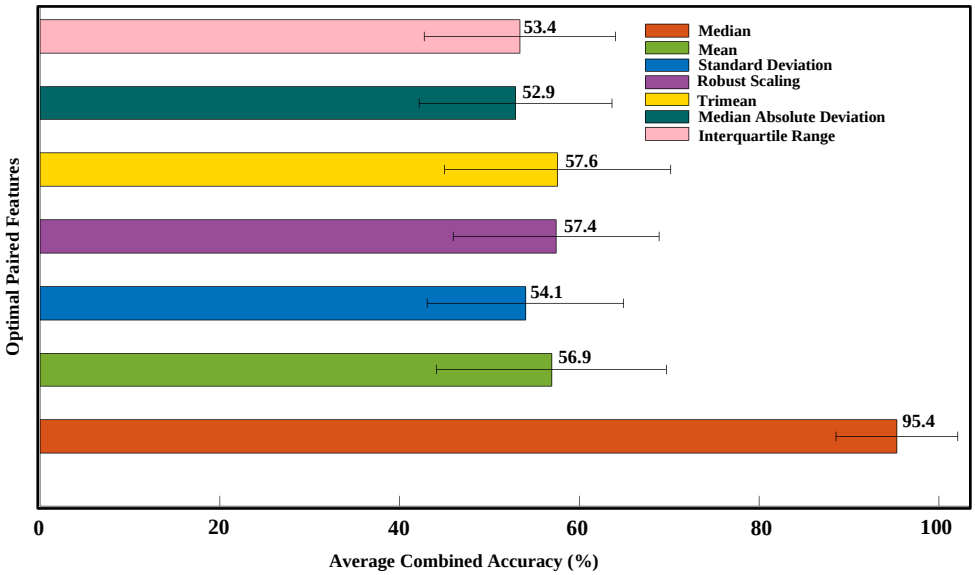

Figure 8. 4: This figure clearly demonstrates that the average combined accuracy varies depending on the threshold computation technique. Specifically, PSD alpha and PSD theta was identified as the optimal combining features for median threshold, while theta/alpha ratio and spectral spread emerged as the optimal combining features for the remaining threshold techniques.

Chapter 9:

DROWSINESS DETECTION AND ALERT SYSTEM

9.1 Autonomous Real-Time Drowsiness Detection and Alert System

Our ultimate aim is to develop a real-time drowsiness detection system for an actual bus (Otokar Kent 290 LF) based on subject-specific pre-calculated EEG feature thresholds obtained in a simulated environment. The system will also include an alert mechanism for the driver using a super silent (66 dB) electro-pneumatic vibrator (Vibco: VS-100) installed at the back of the driver's seat. This alert mechanism will be integrated with the existing bus tire inflation system (TIS). The following steps, as explained in Figure 9. 1, will be followed to successfully accomplish our aim.

9.1.1 Data Acquisition Module (DAM)

Real-time drowsiness detection will begin by capturing the EEG signal from the BrainBit Flex device, which includes four EEG channels that can be placed at any position on the 10-20 scheme. Based on our EEG channel optimization work, we will utilize only one of its EEG channels, positioned at location F4 on the driver's scalp, along with the built-in reference and ground electrodes. The raw EEG signal, in the microvolt range, will be directly captured by the BrainBit Flex, which features dry golden-plated spring-loaded electrodes for optimal signal acquisition. The device has an internal amplifier to enhance the signal-to-noise ratio for better detection and analysis. The amplified signal will be sampled at a rate of 250 Hz and passed through the device's internal filters, with a raw signal bandwidth from 0 Hz to 100 Hz. This processed signal will then be transmitted via Bluetooth Low Energy (BLE) to a laptop running MATLAB. On the laptop, a custom data acquisition program developed with MATLAB's Signal Processing and Instrument Control Toolboxes will interface with the BrainBit Flex's software development kit (SDK). This program will receive the digitized EEG data in real-time through the BLE interface for further processing and analysis.

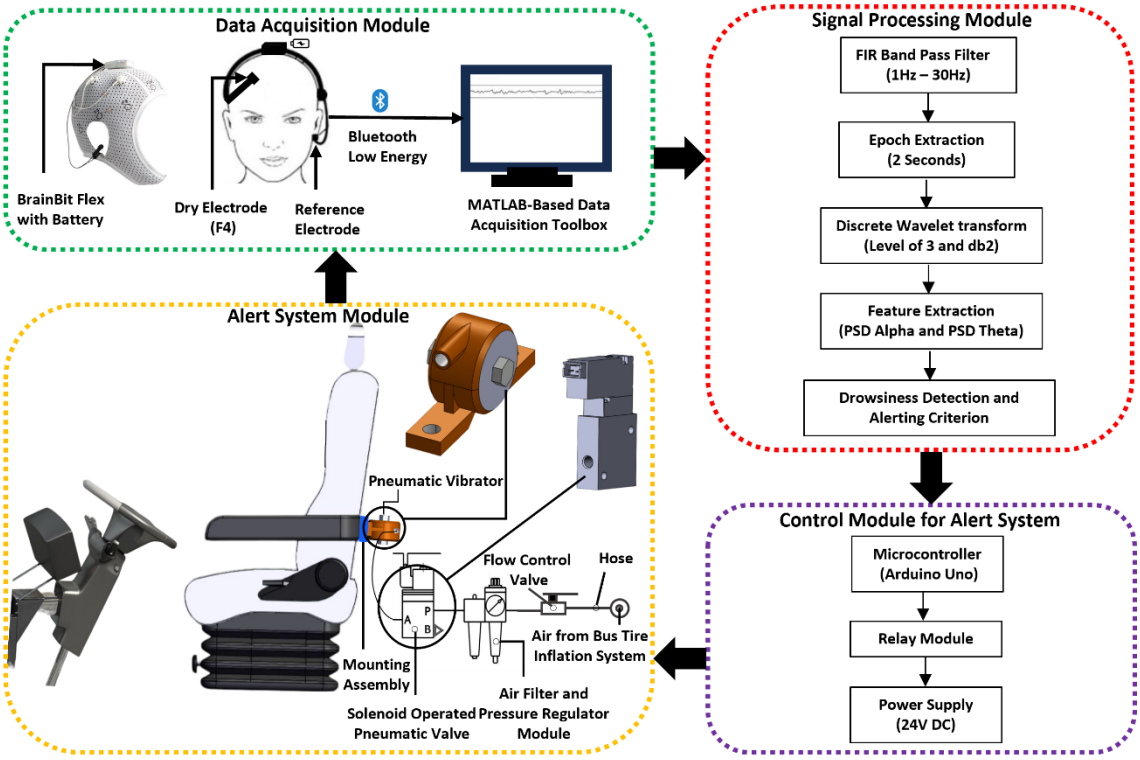

Figure 9. 1: This figure illustrates the autonomous system for real-time driver's drowsiness detection and alertness in an actual bus. Step 1 involves acquiring EEG data from the frontal F4 electrode by using BrainBit Flex EEG device. Step 2 outlines the signal processing technique utilized for drowsiness detection, employing thresholding classification. Step 3 showcases the control system's function in operating the alert system based on input received from Step 2. Finally, Step 4 demonstrates the electro-pneumatic-based alert system designed for the driver.

9.1.2 Signal Processing Module (SPM)

To preprocess the recorded EEG signal, a Finite Impulse Response (FIR) bandpass filter will be employed with lower and higher cutoff frequencies of 1 Hz and 30 Hz, respectively. Subsequently, the signal will be segmented into epochs of 2 seconds each. Discrete Wavelet Transform with a level of 3 and the 'db2' wavelet will then be applied to decompose the signal into four distinct frequency bands: beta, alpha, theta, and delta.

Following decomposition, Power Spectral Density (PSD) values for alpha and theta bands will be calculated for each epoch. These calculated PSD values will then be compared against their predetermined thresholds derived from simulated driving environments based on drowsiness detection and alerting criterion: if the real-time value of PSD alpha falls below its threshold multiplied by 1.15, or if the real-time value of PSD

theta rises above its threshold multiplied by 0.85, MATLAB will generate a digital alert signal.

9.1.3 Control Module for Alert System (CMAS)

MATLAB will communicate with Arduino Uno through a serial connection using Universal Asynchronous Receiver-Transmitter (UART) protocol. MATLAB's Instrument Control Toolbox provides functions to establish serial communication with external devices such as Arduino. A custom MATLAB script will send the digital signal representing drowsiness detection results to Arduino via the serial connection. The signal will be transmitted as a series of bytes, with each byte encoding specific information such as the detection status and any additional parameters.

On the Arduino side, an Arduino program will continuously monitor the serial port for incoming data. Upon receiving the digital signal from MATLAB, Arduino will interpret the data and trigger the appropriate action. In this case, Arduino will control a relay module, which serves as a switch between the microcontroller and the pneumatic valve. When Arduino detects the digital signal indicating drowsiness, it will activate the relay module, allowing power to flow to the solenoid-operated pneumatic valve.

For powering the solenoid-operated pneumatic valve and the relay module, a suitable power supply is required. The solenoid-operated pneumatic valve operates at 24V DC with a power rating of 2.88 W, requiring a current of approximately 120mA. Therefore, the power supply should provide stable 24V DC output with a current rating of at least 120mA to ensure proper operation of the pneumatic valve.

The relay module should be capable of switching the 24V DC power supply to control the pneumatic valve. It should have a voltage rating of 24V DC and a current rating slightly higher than the current required to operate the pneumatic valve, to ensure reliable operation and accommodate any inrush currents. Additionally, the relay module should have a control input compatible with Arduino Uno's digital output pins, which provide 5V logic signals.

Arduino Uno is powered via USB (5V). Its digital output pins can provide 5V logic signals to control the relay module. The Arduino Uno itself consumes very little power, typically around 50-100mA, so the power supply for Arduino Uno does not need to be particularly high-powered.

9.1.4 Alert System Module (ASM)

The alert system module (ASM) will be powered by the compressed air sourced from the tire inflation system (TIS), which operates at a pressure range of 87 to 131 PSI (pounds per square inch). ASM will incorporate a flow control valve (Vibco: 86102) to precisely regulate the flow rate of compressed air coming from the TIS. This controlled airflow will further be purified and regulated its pressure within the range of 29 to 117 PSI by an air filter (5 micron) and pressure regulator module (Vibco: 46102). The air will then be directed to a solenoid-operated 3/2-way, normally closed valve (Festo: MHE2-M1H-3/2G-M7-K), with a nominal flow rate of 100 l/min and a maximum pressure rating of 117 PSI. Upon activation of the pneumatic valve by the relay module, compressed air will be directed to the pneumatic vibrator (VS-100) situated at the back of the driver's seat. The VS-100 operates within a working pressure range of 29-117 PSI and a flow range of 1.5 – 4.0 CFM. The pneumatic vibrator will generate adjustable vibrations within the driver's seat, specifically targeting both armrests, to effectively alert the driver upon detecting drowsiness, thereby enhancing driving safety.

Chapter 10:
CONCLUSION

In this thesis, a high-fidelity bus driving simulator was employed to detect microsleep (MS) and drowsiness in drivers with Obstructive Sleep Apnea (OSA). First, we successfully identified microsleep (MS) by correlating driving attributes (off-road and on-road episodes) with EEG signals, specifically by recognizing the theta/alpha ratio as a novel indicator, which decreases when a person experiences MS compared to alert episodes. Secondly, we successfully identified drowsiness by correlating EEG signals with visual-based signals derived from facial video recordings while driving. Specifically, we recognized delta/alpha and delta/theta ratios as novel indicators, which decrease when a person becomes drowsy, alongside the theta/alpha ratio. Thirdly, we optimized a 6-channel EEG (F4, F3, C4, C3, O1, and O2) system to a single-channel EEG (F4) system by pairing optimal features (PSD alpha and PSD theta), which identified drowsiness episodes slightly better than a multichannel system. Fourthly, we presented an autonomous system for real-time drowsiness detection and alertness in an actual bus environment using the single channel EEG (F4) system. To alert the driver, we proposed an electro-pneumatic vibrator that produces adjustable vibrations upon drowsiness detection within the driver's seat, utilizing compressed air coming from the existing bus tire inflation system. In conclusion, our work could potentially be employed to assess fitness-to-drive in OSA patients using a driving simulator, reduce hardware and computational demands, and pave the way for an effective real-time drowsiness detection and alert system for actual bus drivers.

Future research should explore the algorithm to integrate the three signals (EEG, vehicle-based, and visual-based) while considering the natural lag between these signals to effectively capture the entire microsleep and drowsiness episodes. Additionally, future research should apply our proposed real-time drowsiness detection and alertness methodology to evaluate its efficacy in practical settings, potentially contributing to the development of intelligent vehicles.

BIBLIOGRAPHY

[1] D. P. White, "Sleep apnea," Proceedings of the American Thoracic Society, vol. 3, no. 1, pp. 124-128, Jan. 2006.

[2] R. Heinzer et al., "Prevalence of sleep-disordered breathing in the general population: The HypnoLaus study," Lancet Respir. Med., vol. 3, no. 4, pp. 310-318, Apr. 2015.

[3] A. Malhotra and D. White, "Seminar: Obstructive Sleep Apnoea," Lancet, vol. 360, pp. 237-245, Jul. 2002.

[4] H. Greenberg, V. Lakticova, S. M. Scharf, "Obstructive Sleep Apnea: Clinical Features, Evaluation, and Principles of Management," in Principles and Practice of Sleep Medicine (Sixth Edition), Eds. M. Kryger, T. Roth, W. C. Dement, Elsevier, 2017, pp. 1110-1124.e6.

[5] W. De Backer, "Obstructive sleep apnea/hypopnea syndrome," Panminerva Med., vol. 55, no. 2, pp. 191-195, Jun. 2013.

[6] D. J. Eckert et al., "Central sleep apnea: pathophysiology and treatment," Chest, vol. 131, no. 2, pp. 595-607, Feb. 2007.

[7] A. B. Hernandez and S. P. Patil, "Pathophysiology of central sleep apneas," Sleep Breath, vol. 20, no. 2, pp. 467-482, May 2016.

[8] P. E. Peppard et al., "Increased prevalence of sleep-disordered breathing in adults," Am. J. Epidemiol., vol. 177, pp. 1006-1006, 2013.

[9] A. V. Benjafield et al., "Estimation of the global prevalence and burden of obstructive sleep apnoea: a literature-based analysis," Lancet Respir. Med., vol. 7, pp. 687-687, 2019.

[10] L. M. Donovan and V. K. Kapur, "Prevalence and Characteristics of Central Compared to Obstructive Sleep Apnea: Analyses from the Sleep Heart Health Study Cohort," Sleep, vol. 39, p. 1353, 2016.

[11] E. M. Balk et al., "Diagnosis and Treatment of Obstructive Sleep Apnea in Adults," Comparative Effectiveness Reviews, no. 32, Agency for Healthcare Research and

Quality (US), Rockville, MD, Jul. 2011. Available: https://www.ncbi.nlm.nih.gov/books/NBK63560/

[12] C. Lal et al., "Excessive Daytime Sleepiness in Obstructive Sleep Apnea: Mechanisms and Clinical Management," Ann. Am. Thorac. Soc., vol. 18, no. 5, pp. 757-768, May 2021.

[13] P. M. Macey et al., "Relationship between obstructive sleep apnea severity and sleep, depression and anxiety symptoms in newly diagnosed patients," PLoS One, vol. 5, no. 4, p. e10211, Apr. 2010.

[14] T. L. T. Silveira et al., "Automated drowsiness detection through wavelet packet analysis of a single EEG channel," Expert Systems with Applications, vol. 55, pp. 559-565, 2016.

[15] E. Morrone et al., "Microsleep as a marker of sleepiness in obstructive sleep apnea patients," J. Sleep Res., vol. 29, no. 2, p. e12882, Apr. 2020.

[16] M. T. R. Peiris et al., "Detecting behavioral microsleeps from EEG power spectra," in Proceedings of the International Conference of the IEEE Engineering in Medicine and Biology Society, pp. 5723-5726, 2006.

[17] J. Skorucak et al., "Automatically detected microsleep episodes in the fitness-to-drive assessment," Front. Neurosci., vol. 14, p. 8, 2020.

[18] J. Skorucak et al., "Automatic detection of microsleep episodes with feature-based machine learning," Sleep, vol. 43, no. 1, p. zsz225, 2020.

[19] R. J. Buckley et al., "Attention lapses and behavioural microsleeps during tracking, psychomotor vigilance, and dual tasks," Conscious. Cogn., vol. 45, pp. 174-183, 2016.

[20] P. R. Davidson, R. D. Jones, and M. T. R. Peiris, "EEG-based lapse detection with high temporal resolution," IEEE Trans. Biomed. Eng., vol. 54, no. 5, pp. 832-839, May 2007.

[21] R. Shoorangiz et al., "Detection and Prediction of Microsleeps from EEG using Spatio-Temporal Patterns," in 2019 41st Annual International Conference of the IEEE

Engineering in Medicine and Biology Society (EMBC), Berlin, Germany, 2019, pp. 522-525.

[22] A. Malafeev et al., "Automatic Detection of Microsleep Episodes with Deep Learning," Front. Neurosci., vol. 15, p. 564098, Mar. 2021.

[23] G. Miyama et al., "Risk factors for collisions and near-miss incidents caused by drowsy bus drivers," Int. J. Environ. Res. Public Health, vol. 17, no. 12, p. 4370, Jun. 2020.

[24] S. Saleem, "Risk assessment of road traffic accidents related to sleepiness during driving: a systematic review," East Mediterr. Health J., vol. 28, no. 9, pp. 695-700, 2022.

[25] M. R. Bonsignore et al., "Epidemiology, Physiology and Clinical Approach to Sleepiness at the Wheel in OSA Patients: A Narrative Review," J. Clin. Med., vol. 11, no. 13, pp. 3691, Jun. 2022.

[26] M. E. Howard et al., "Sleepiness, sleep disordered breathing, and accident risk factors in commercial vehicle drivers," Am. J. Respir. Crit. Care Med., vol. 170, pp. 1014–1021, 2004.

[27] S. Tregear et al., "Obstructive sleep apnea and risk of motor vehicle crash: systematic review and meta-analysis," J. Clin. Sleep Med., vol. 5, no. 6, pp. 573-581, Dec. 2009.

[28] O. M. Qureshi et al., "Ahmedpur Sharqia oil tanker tragedy: Lessons learnt from one of the biggest road accidents in history," J. Loss Prevention Process. Ind., vol. 67, Art. no. 104243, Sep. 2020.

[29] Drivers are Falling Asleep Behind the Wheel" [Website]. NSC: National Safety Council. [Online]. Available: https://www.nsc.org/road/safety-topics/fatigued-driver. Accessed on: Jun. 07, 2023.

[30] The Prevalence and Impact of Drowsy Driving," AAA Foundation, [Online]. Available: https://aaafoundation.org/prevalence-impact-drowsy-driving/. [Accessed: April 2024].

[31] L. E. Krahn et al., "Recommended protocols for the Multiple Sleep Latency Test and Maintenance of Wakefulness Test in adults: guidance from the American Academy of Sleep Medicine," J Clin Sleep Med, vol. 17, no. 12, pp. 2489-2498, Dec. 2021.

[32] D.R. Schreier et al., "Driving simulators in the clinical assessment of fitness to drive in sleepy individuals: a systematic review," Sleep Medicine Reviews, vol. 38, pp. 86-100, 2018.

[33] F. Pizza et al., "Daytime Sleepiness and Driving Performance in Patients with Obstructive Sleep Apnea: Comparison of the MSLT, the MWT, and a Simulated Driving Task," Sleep, vol. 32, pp. 382–391, 2009.

[34] H.J. Moller et al., "Simulator Performance, Microsleep Episodes, and Subjective Sleepiness: Normative Data Using Convergent Methodologies to Assess Driver Drowsiness," J. Psychosom. Res., vol. 61, pp. 335–342, 2006.

[35] L.N. Boyle et al., "Driver Performance in the Moments Surrounding a Microsleep," Transp. Res. Part F Traffic Psychol. Behav., vol. 11, pp. 126–136, 2008.

[36] M.R. Risser and J.C. Ware, "Driving Simulation with EEG Monitoring in Normals and Obstructive Sleep Apnea Patients," Annu. Proc. Assoc. Adv. Automot. Med., vol. 43, pp. 317–328, 1999.

[37] K. Fujiwara et al., "Heart Rate Variability-Based Driver Drowsiness Detection and Its Validation With EEG," IEEE Trans. Biomed. Eng., vol. 66, pp. 1769–1778, 2019.

[38] S.A. El-Nabi et al., "Machine Learning and Deep Learning Techniques for Driver Fatigue and Drowsiness Detection: A Review," Multimed. Tools Appl., vol. 83, pp. 9441–9477, 2024.

[39] T. Nguyen et al, "Utilization of a Combined EEG/NIRS System to Predict Driver Drowsiness," Sci. Rep., vol. 7, article no. 43933, 2017.

[40] W.-B. Horng et al., "Driver Fatigue Detection Based on Eye Tracking and Dynamic Template Matching," in Proceedings of the IEEE International Conference on Networking, Sensing and Control, Taipei, Taiwan, pp. 7–12, 21–23 March 2004.

[41] İ. Umut, O. Aki, E. Uçar, and L. Öztürk, "Detection of Driver Sleepiness and Warning the Driver in Real-Time Using Image Processing and Machine Learning Techniques," Adv. Sci. Technol. Res. J., vol. 11, pp. 95–102, 2017.

[42] N. Alioua, A. Amine, and M. Rziza, "Driver's Fatigue Detection Based on Yawning Extraction," Int. J. Veh. Technol., vol. 2014, article ID 678786, 2014.

[43] A. Mittal et al., "Head Movement-Based Driver Drowsiness Detection: A Review of State-of-Art Techniques," in 2016 IEEE International Conference on Engineering and Technology (ICETECH), Coimbatore, India, pp. 903–908, 17–18 March 2016.

[44] A.D. McDonald et al., "Steering in a Random Forest: Ensemble Learning for Detecting Drowsiness-Related Lane Departures," Hum. Factors, vol. 56, pp. 986–998, 2014.

[45] S. Arefnezhad et al., "Applying Deep Neural Networks for Multi-level Classification of Driver Drowsiness Using Vehicle-based Measures," Expert Syst. Appl., vol. 162, article ID 113778, 2020.

[46] M. R. Risser and J. C. Ware, "Driving Simulation with EEG Monitoring in Normals and Obstructive Sleep Apnea Patients," Annu. Proc. Assoc. Adv. Automot. Med., vol. 43, pp. 317-328, 1999.

[47] H. J. Moller et al., "Simulator performance, microsleep episodes, and subjective sleepiness: normative data using convergent methodologies to assess driver drowsiness," J Psychosom Res, vol. 61, no. 3, pp. 335-342, Sep. 2006.

[48] A. Paul, L. Boyle, J. Tippin, and M. Rizzo, "Variability of Driving Performance During Microsleeps," in Driving Assessment Conference 3(2005), 2005, pp. 18-24, doi: 10.17077/drivingassessment.1138.

[49] G. Lenis et al., "Detection of microsleep events in a car driving simulation study using electrocardiographic features," Current Directions in Biomedical Engineering, vol. 2, no. 1, pp. 283-287, 2016.

[50] Y.-S. Kweon et al., "Automatic micro-sleep detection under car-driving simulation environment using night-sleep EEG," 2020, arXiv:2012.05705.

[51] A. Hertig-Godeschalk et al., "Microsleep episodes in the borderland between wakefulness and sleep," Sleep, vol. 43, no. 1, 2020.

[52] O. Shechtman et al., "Comparison of driving errors between on-the-road and simulated driving assessment: a validation study," Traffic Injury Prevention, vol. 10, no. 4, 2009, pp. 379-385.

[53] R.A. Wynne, V. Beanland, and P.M. Salmon, "Systematic review of driving simulator validation studies," Safety Science, vol. 117, pp 138-151, 2019.

[54] C. Guilleminault et al., "Altered states of consciousness in disorders of daytime sleepiness," Journal of the Neurological Sciences, vol. 26, no. 3, pp. 377-393, 1975.

[55] M.K. Hussein et al., "Driver Drowsiness Detection Techniques: A Survey," in 2021 1st Babylon International Conference on Information Technology and Science (BICITS), Babil, Iraq, pp. 45–51, 28–29 April 2021.

[56] S. Arefnezhad et al., "Driver Drowsiness Detection Based on Steering Wheel Data Applying Adaptive Neuro-Fuzzy Feature Selection," Sensors, vol. 19, article ID 943, 2019.

[57] S. Soares, S. Ferreira, and A. Couto, "Driving Simulator Experiments to Study Drowsiness: A Systematic Review," Traffic Inj. Prev., vol. 21, pp. 29–37, 2020.

[58] S. Arefnezhad et al., "Driver Drowsiness Estimation Using EEG Signals with a Dynamical Encoder-Decoder Modeling Framework," *Sci. Rep.*, vol. 12, article ID 2650, 2022.

[59] R.C.-H. Chang et al., "Drowsiness Detection System Based on PERCLOS and Facial Physiological Signal," Sensors, vol. 22, article ID 5380, 2022.

[60] L. Lang and H. Qi, "The Study of Driver Fatigue Monitor Algorithm Combined PERCLOS and AECS," in Proceedings of the 2008 International Conference on Computer Science and Software Engineering, Wuhan, China, pp. 349–352, 12–14 December 2008.

[61] J.-F. Xie, M. Xie, and W. Zhu, "Driver Fatigue Detection Based on Head Gesture and PERCLOS," in Proceedings of the 2012 International Conference on Wavelet

Active Media Technology and Information Processing (ICWAMTIP), Chengdu, China, pp. 128–131, 17–19 December 2012.

[62] W. Liu, H. Sun, and W. Shen, "Driver Fatigue Detection Through Pupil Detection and Yawning Analysis," in Proceedings of the 2010 International Conference on Bioinformatics and Biomedical Technology, Chengdu, China, pp. 404–407, 16–18 April 2010.

[63] B. Cheng et al., "Driver Drowsiness Detection Based on Multi-Source Information," Hum. Factors Ergon. Manuf. Serv. Ind., vol. 22, pp. 450–467, 2012.

[64] R.J. Hanowski et al., "PERCLOS+: Development of a Robust Field Measure of Driver Drowsiness," in Proceedings of the 15th World Congress on Intelligent Transport Systems and ITS America's 2008 Annual Meeting, New York, NY, USA, 16–20 November 2008.

[65] J.S. Bajaj et al., "System and Method for Driver Drowsiness Detection Using Behavioral and Sensor-Based Physiological Measures," Sensors, vol. 23, article ID 1292, 2023.

[66] T. Danisman, I.M. Bilasco, C. Djeraba, and N. Ihaddadene, "Drowsy Driver Detection System Using Eye Blink Patterns," in Proceedings of the 2010 International Conference on Machine and Web Intelligence, Algiers, Algeria, pp. 230–233, 3–5 October 2010.

[67] J. LaRocco, M.D. Le, and D.-G. Paeng, "A systemic review of available low-cost EEG headsets used for drowsiness detection," Frontiers in Neuroinformatics, vol. 14, Oct. 2020.

[68] P. Sawangjai et al., "Consumer Grade EEG Measuring Sensors as Research Tools: A Review," IEEE Sensors Journal, vol. 20, no. 8, pp. 3996-4024, Apr. 15, 2020.

[69] C.-T. Lin et al., "A real-time wireless brain–computer interface system for drowsiness detection", IEEE Trans. Circuits Syst., vol. 4, no. 4, pp. 214-222, Aug. 2010.

[70] Y. Punsawad et al., "Weighted-frequency index for EEG-based mental fatigue alarm system," International Journal of Applied Biomedical Engineering, vol. 4, no. 1, pp. 36-41, Apr. 2011.

[71] B. Van Hal et al, "Low-cost EEG-based sleep detection," in Proceedings of the 36th Annual International Conference of the IEEE Engineering in Medicine and Biology Society (EMBC), pp. 4571-4574, Aug. 2014.

[72] G. Li, B. -L. Lee and W. -Y. Chung, "Smartwatch-Based Wearable EEG System for Driver Drowsiness Detection," in IEEE Sensors Journal, vol. 15, no. 12, pp. 7169-7180, Dec. 2015.

[73] M. Ogino and Y. Mitsukura, "Portable Drowsiness Detection through Use of a Prefrontal Single-Channel Electroencephalogram," Sensors (Basel), vol. 18, no. 12, p. 4477, Dec. 2018.

[74] W.M. Shalash, "Driver Fatigue Detection with Single EEG Channel Using Transfer Learning," in 2019 IEEE International Conference on Imaging Systems and Techniques (IST), Abu Dhabi, United Arab Emirates, pp. 1-6, 2019.

[75] R. Minhas et al., "A Novel Approach to Quantify Microsleep in Drivers with Obstructive Sleep Apnea by Concurrent Analysis of EEG Patterns and Driving Attributes," in IEEE Journal of Biomedical and Health Informatics, vol. 28, no. 3, pp. 1341-1352, March 2024.

[76] R. Minhas et al., "Association of Visual-Based Signals with Electroencephalography Patterns in Enhancing the Drowsiness Detection in Drivers with Obstructive Sleep Apnea," Sensors, vol. 24, no. 9, p. 2625, 2024.

[77] H. J. Eoh, M. K. Chung and S. H. Kim, "Electroencephalographic studyof drowsiness in simulated driving with sleep deprivation", Int. J. Ind. Ergonom., vol. 35, pp. 307-320, 2005.

[78] C. -T. Lin et al., "A Real-Time Wireless Brain–Computer Interface System for Drowsiness Detection," in *IEEE Transactions on Biomedical Circuits and Systems*, vol. 4, no. 4, pp. 214-222, Aug. 2010.

[79] G. Klem et al., "The ten-twenty electrode system of the International Federation of Clinical Neurophysiology," Electroencephalography and Clinical Neurophysiology Supplementary, vol. 52, pp. 3-6, 1993.

[80] C. Papadelis et al., "Indicators of Sleepiness in an ambulatory EEG study of night driving," in 2006 International Conference of the IEEE Engineering in Medicine and Biology Society, New York, NY, USA, 2006, pp. 6201-6204.

[81] C.-T. Lin et al., "EEG-Based Drowsiness Estimation for Safety Driving Using Independent Component Analysis," IEEE Trans. Circuits Syst. I Regul. Pap., vol. 52, pp. 2726–2738, 2005.

[82] Y. Li, L. Shen, M. Sun, "Electroencephalography Study of Frontal Lobe Evoked by Dynamic Random-Dot Stereogram," Invest Ophthalmol Vis Sci, vol. 63, no. 5, p. 7, May 2022.

[83] L. J. Epstein et al., "Clinical guideline for the evaluation, management and long-term care of obstructive sleep apnea in adults," J Clin Sleep Med, vol. 5, no. 3, pp. 263-276, Jun. 2009.

[84] J. K. Walsh et al., "Effect of caffeine on physiological sleep tendency and ability to sustain wakefulness at night," Psychophysiology, vol. 101, pp. 271-273, 1990.

[85] A. Chougule et al., "Enabling Safe ITS: EEG-Based Microsleep Detection in VANETs," in IEEE Transactions on Intelligent Transportation Systems, 2022.

[86] R.J. Buckley et al., "Attention lapses and behavioral microsleeps during tracking, psychomotor vigilance, and dual tasks," Consciousness and Cognition, vol. 45, pp. 174-183, 2016.

[87] A. Mortazavi et al., "Effect of drowsiness on driving performance variables of commercial vehicle drivers," International Journal of Automotive Technology, vol. 10, pp. 391-404, 2009

[88] T.A. Ranney, "Psychological fidelity: perception of risk," in D.L. Fisher, M. Rizzo, J.K. Caird, and J.D. Lee (Eds.), Handbook of Driving Simulation for Engineering, Medicine, and Psychology, CRC Press, Boca Raton, FL, 2012, pp. 9:1-13.

[89] S. Kristiansen et al., "Comparing manual and automatic scoring of sleep monitoring data from portable polygraphy," J. Sleep Res., vol. 30, no. 2, p. e13036, Apr. 2021.

[90] Y. Harrison and J.A. Horne, "Occurrence of 'microsleeps' during daytime sleep onset in normal subjects," Electroencephalography and Clinical Neurophysiology, vol. 98, no. 5, pp. 411-416, 1996.

[91] P. Sauseng et al., "Dissociation of sustained attention from central executive functions: local activity and interregional connectivity in the theta range," Eur J Neurosci, vol. 25, pp. 587-593, 2007.

[92] J. Liu et al., "Sustaining Attention for a Prolonged Duration Affects Dynamic Organizations of Frequency-Specific Functional Connectivity," Brain Topogr, vol. 33, no. 6, pp. 677-692, Nov 2020.

[93] P. Dobrakowski et al., "Changes in the Electrical Activity of the Brain in the Alpha and Theta Bands during Prayer and Meditation," Int J Environ Res Public Health, vol. 17, no. 24, p. 9567, Dec 2020.

[94] Mercy, M. Stella. "Performance analysis of epileptic seizure detection using DWT & ICA with neural networks." Int. J. Comput. Eng. Res., vol. 2, no. 4, pp. 1109-1113, 2012.

[95] M. Riera-Guasp et al., "A General Approach for the Transient Detection of Slip-Dependent Fault Components Based on the Discrete Wavelet Transform," IEEE Trans. Ind. Electron., vol. 55, no. 12, pp. 4167-4180, Dec. 2008.

[96] N.K. Al-Qazzaz et al., "Automatic Artifact Removal in EEG of Normal and Demented Individuals Using ICA-WT during Working Memory Tasks," Sensors (Basel), vol. 17, no. 6, p. 1326, Jun. 2017.

[97] C. Polat and M.S. Özerdem, "Introduction to Wavelets and their applications in signal denoising," Bitlis Eren University Journal of Science and Technology, vol. 8, no. 1, pp. 1-10, Jun. 2018.

[98] B. S. Nanthini and B. Santhi, "Electroencephalogram Signal Classification for Automated Epileptic Seizure Detection Using Genetic Algorithm," J. Nat. Sci. Biol. Med., vol. 8, no. 2, pp. 159-166, Jul.-Dec. 2017.

[99] A. Tavakoli Kashani, M. Rakhshani Moghadam, and S. Amirifar, "Factors affecting driver injury severity in fatigue and drowsiness accidents: a data mining framework," J. Inj. Violence Res., vol. 14, no. 1, pp. 75-88, Jan. 2022.

[100] L. Meuleners et al., "Obstructive Sleep Apnea, Health-Related Factors, and Long-Distance Heavy Vehicle Crashes in Western Australia: A Case-Control Study," J Clin Sleep Med., vol. 11, pp. 413-418, 2015.

[101] R. Heinzer et al., "Prevalence of Sleep-Disordered Breathing in the General Population: The HypnoLaus Study," Lancet Respir Med., vol. 3, pp. 310-318, 2015.

[102] P.E. Peppard et al., "Increased Prevalence of Sleep-Disordered Breathing in Adults," Am J Epidemiol., vol. 177, pp. 1006-1014, 2013.

[103] J. Connor et al., "Driver Sleepiness and Risk of Serious Injury to Car Occupants: Population-Based Case-Control Study," BMJ, vol. 324, p. 1125, 2002.

[104] P. Viola and M. Jones, "Rapid Object Detection Using a Boosted Cascade of Simple Features," in Proceedings of the 2001 IEEE Computer Society Conference on Computer Vision and Pattern Recognition (CVPR 2001), Kauai, HI, USA, pp. I-I, 8–14 December 2001.

[105] D.E. King, "Dlib-ml: A Machine Learning Toolkit," J. Mach. Learn. Res., vol. 10, pp. 1755-1758, 2009.

[106] A. Zaki et al., "Fatigue Detection among Operators in Industry Based on Euclidean Distance Computation Using Python Software," Int. J. Emerg. Trends Eng. Res., vol. 8, pp. 6375-6379, 2020.

[107] S. Sathasivam et al., "Drowsiness Detection System Using Eye Aspect Ratio Technique," in 2020 IEEE Student Conference on Research and Development (SCOReD), Batu Pahat, Malaysia, pp. 448-452, 27–29 September 2020.

[108] F. You et al., "A Real-time Driving Drowsiness Detection Algorithm with Individual Differences Consideration," IEEE Access, vol. 7, pp. 179396-179408, 2019.

[109] C. Dewi et al., "Eye Aspect Ratio for Real-Time Drowsiness Detection to Improve Driver Safety," Electronics, vol. 11, article ID 3183, 2022.

[110] Q. Cheng et al., "Assessment of Driver Mental Fatigue Using Facial Landmarks," IEEE Access, vol. 7, pp. 150423-150434, 2019.

[111] Y. Wang, S.S. Toor, R. Gautam, and D.B. Henson, "Blink Frequency and Duration During Perimetry and Their Relationship to Test-Retest Threshold Variability," Invest. Ophthalmol. Vis. Sci., vol. 52, pp. 4546-4550, 2011.

[112] W.A. Mir et al., "Deep-EEG: An Optimized and Robust Framework and Method for EEG-Based Diagnosis of Epileptic Seizure," Diagnostics, vol. 13, article ID 773, 2023.

[113] I. Aliyu and C.G. Lim, "Selection of Optimal Wavelet Features for Epileptic EEG Signal Classification with LSTM," Neural Comput. Appl., vol. 35, pp. 1077–1097, 2023.

[114] I. Güler and E.D. Übeyli, "Adaptive Neuro-Fuzzy Inference System for Classification of EEG Signals Using Wavelet Coefficients," J. Neurosci. Methods, vol. 148, no. 2, pp. 113–121, 2005.

[115] N. Sriraam, T.K. Padma Shri, and U. Maheshwari, "Recognition of Wake-Sleep Stage 1 Multichannel EEG Patterns Using Spectral Entropy Features for Drowsiness Detection," Australas Phys Eng Sci Med, vol. 39, pp. 797-806, 2016.

[116] P. Krishnan, S. Yaacob, and A.P. Krishnan, "Drowsiness Detection Using Electroencephalogram Anomaly Based on Spectral Entropy Features and Linear Classifier," in M. Abu Bakar, F. Azwa Zamri, A. Öchsner (Eds.), Progress in Engineering Technology II, Advanced Structured Materials, vol. 131, Springer, Cham, 2020.

[117] T. Giannakopoulos and A. Pikrakis, Introduction to Audio Analysis, Academic Press, February 2014, ISBN: 9780080993898. Available online: https://www.oreilly.com/library/view/introduction-to-audio/9780080993881/ (accessed on 1 April 2023).

[118] J.C. De Winter, S.D. Gosling, and J. Potter, "Comparing the Pearson and Spearman Correlation Coefficients Across Distributions and Sample Sizes: A Tutorial Using Simulations and Empirical Data," Psychol. Methods, vol. 21, no. 3, pp. 273–290, 2016.